This is a preprint, the final version is subject to change, of the American Mineralogist (MSA)
Cite as Authors (Year) Title. American Mineralogist, in press.
DOI: https://doi.org/10.2138/am-2019-6652

Revision 2: submission to *American Mineralogist*.

Spinel-Anorthosites on the Moon: Impact Melt Origins Suggested by Enthalpy Constraints

Allan H. Treiman[1], Michael J. Kulis[2], and Allen F. Glazner[3]

[1] Lunar and Planetary Institute – Universities Space Research Association, 3600 Bay Area Boulevard, Houston, TX 77058. treiman@lpi.usra.edu

[2] Extreme Environments Laboratory, NASA Glenn Research Center, 2100 Brookpark Road, Cleveland, OH 44135. Michael.J.Kulis@nasa.gov

[3] Department of Geological Sciences, University of North Carolina, Chapel Hill, NC 27599. afg@unc.edu

Abstract

Magnesium aluminate spinel, $(Mg,Fe)Al_2O_4$, is uncommon in lunar rocks, but petrologically significant. Recent near-infrared spectra of the Moon have delineated regions where spinel is the only ferromagnesian mineral; the rock is inferred to be spinel anorthosite. One hypothesis is that significant pressure is required for spinel formation; another is that spinel-bearing rocks form by low-pressure assimilation of highlands anorthosite into olivine-rich basaltic (i.e., picritic) magmas. Here, we evaluate the heat (i.e., enthalpy) required for this assimilation process. Magma compositions are the picritic Apollo 14 B green glass, and an estimate for the magma parental to Mg-Suite cumulate rocks. From calculated enthalpy-composition phase diagrams, assimilation of anorthite into either magma cannot produce spinel

anorthosite unless the anorthite is already hotter than ~1300°C. For cooler anorthosite, assimilation will produce olivine- and/or pyroxene-bearing rocks. Such hot anorthite could be produced by nearby passage of large volumes of magma, but this is not obviously consistent with occurrences of spinel far from outcrops of basaltic rocks. Hot anorthosite could also be produced by global tidal flexure; that mechanism could have only been efficient early in lunar history when a solid anorthosite crust floated above an evolved magma ocean, and it is not clear how picritic magma could pass through the magma ocean to interact with anorthite in the crust. On the other hand, spinel-bearing anorthosite can form directly on cooling of superliquidus melts of anorthite-rich composition. Such superliquidus melts can be generated by impact events; this mechanism seems likely, given the Moon's: ubiquity of impact craters, abundance of impact-metamorphosed lunar rocks, and common presence in lunar regolith of impact glasses (quenched superliquidus impact melts) of appropriate compositions. High pressure does stabilize spinel in basaltic and peridotitic systems, but available models do not permit quantitative evaluation of the effects of pressure on the enthalpy required for assimilation. Near the lunar surface, the most likely process of spinel formation is rapid crystallization of impact melts of anorthosite + picrite or peridotite compositions. The presence of spinel anorthosite on the walls and central peaks of impact craters results from rapid cooling and partial crystallization of superliquidus melts produced in the impacts, and not from uplift of deep material to the Moon's surface.

.

This is a preprint, the final version is subject to change, of the American Mineralogist (MSA)
Cite as Authors (Year) Title. American Mineralogist, in press.
DOI: https://doi.org/10.2138/am-2019-6652

Introduction

Magnesian aluminate spinel, $(Mg,Fe)Al_2O_4$ or spinel-hercynite solid solution, is an uncommon constituent of lunar rocks, both among returned samples and lunar meteorites. In recent years, orbital remote sensing data have shown that spinel is widespread across the lunar highlands, and these new findings have reignited debate about the origin and significance of lunar spinel. Did spinel-bearing rocks form at high pressure, as do terrestrial spinel peridotites? Did spinel-bearing rocks form by assimilation of crustal anorthosite into picritic magmas? Did spinel-bearing rocks form as products of impact melting and mixing? In this work, we have investigated the constraints that heats (i.e., enthalpies) of melting place on the latter two hypotheses, following Bowen (1922) and Bowen (1928).

Lunar Mg-Fe Aluminate Spinel

Magnesian aluminate spinels (*sensu stricto*) are widespread but rare in feldspathic lunar rocks; we do not consider spinels rich in chromite (Cr) and ulvöspinel (Ti) components, which are common in lunar mare basalts. Most lunar aluminate spinels are pinkish or purplish in hand sample or thin section, reflecting small proportions of Cr substituting for Al (Williams et al., 2016). This color is the basis for rock names like “pink spinel troctolite” (Prinz et al., 1973; Mehta and Goldstein, 1980), and “pink spinel anorthosite” (Pieters et al., 2011), although the rocks themselves are not pink.

Aluminate spinel in lunar rocks occurs in several petrographic and geological settings: as mineral fragments in regolith breccias, in cumulate igneous rocks, in cataclasites with evidence of equilibration at high pressure, and in impact melts and crystalline impact melt breccias. Spinel is abundant in several lunar troctolites (olivine-plagioclase rocks), most notably (Figs. 1 a-c) in Apollo 16 sample 67435 (Prinz et al., 1973), Apollo 15 sample 15295,101 (Marvin et al., 1989),

and in lunar meteorites including NWA 482 and Dho 489 (Daubar et al., 2002; Takeda et al., 2006). In these troctolites, pink spinel occurs as rounded equant grains enclosed in olivine, plagioclase, or cordierite. Many lunar breccias and regolith samples contain isolated grains of spinel, which could reasonably be derived from spinel troctolites, e.g. ALH 81005 and NWA 5744 (Gross and Treiman, 2011; Robinson and Kring, 2018).

Spinel is present in several lunar cataclastic rocks, which are inferred to be annealed impact breccias (Fig. 1d). Most cataclasites are troctolitic, and rarely contain aluminous orthopyroxene or cordierite (Herzberg, 1978; Baker and Herzberg, 1980; Herzberg and Baker, 1980; Eckert et al., 1991; Nazarov et al., 2011). In these mineral assemblages, the alumina content of pyroxene increases with equilibration pressure (Herzberg, 1983), in the range of 0.1-0.2 GPa (Herzberg, 1983; McCallum and Schwartz, 2001; Nazarov et al., 2011).

Finally, spinel is present in many lunar impact melt rocks, crystalline impact-melt breccias, and in fragments of such in other breccias (Figs. 1d-f) (Christophe-Michel-Levy et al., 1972; Walker et al., 1973; Delano, 1977; McGee et al., 1977; James and Hedenquist, 1978; Marvin and Walker, 1985; Daubar et al., 2002; Treiman et al., 2010; Gross and Treiman, 2011; Demidova et al., 2017). The partially melted troctolite fragment in 12033,618 (Marvin and Walker, 1985), Figure 1e, shows that spinel can be the first solid phase to form from melted olivine + plagioclase (Irvine, 1974). In many impact melt breccias, spinel grains are completely enclosed by plagioclase and/or olivine (Figs. 1d, e), which is also consistent with this mechanism.

Interest in lunar spinel has been revived by orbital near-infrared spectroscopic mapping by instruments on the Chandraya'an and Kaguya spacecraft (Haruyama et al., 2008; Pieters et al., 2009). Ferrous iron in $(Mg,Fe)Al_2O_4$ spinel has a strong distinctive absorption band from ~2 μm

to longer wavelengths (Cloutis et al., 2004; Pieters et al., 2011; Gross et al., 2014; Jackson et al., 2014; Williams et al., 2016), and this band is prominent in reflectance spectra of many walls and central peaks of impact craters across the Moon (Dhingra et al., 2011; Pieters et al., 2011; Kaur et al., 2012; Lal et al., 2012; Dhingra et al., 2013; Pieters et al., 2014; Prissel et al., 2014; Sun et al., 2017). Surprisingly, these remote-sensing detections of spinel cannot be related to known lunar samples because they show little spectral evidence of olivine or pyroxene, i.e. they cannot be 'pink spinel' troctolites or peridotites. Because of this absence of olivine and pyroxene, these spectra are inferred to represent spinel-bearing anorthosites (Pieters et al., 2011), called pink spinel anorthosites or PSA.

Origins of Lunar Spinel

With lunar spinels in such a range of petrographic and geologic settings, it is not surprising that a range of origins has been proposed. The earliest descriptions of spinel troctolites emphasized their Al-rich bulk compositions, and suggested that they represented spinel cumulates from aluminous basaltic magmas (Prinz et al., 1973; Marvin et al., 1989). However, the parentage of such aluminous, troctolitic basaltic magmas is not clear (Hess, 1994; Ariskin, 2007; Prissel and Gross, 2018).

High pressure stabilizes spinel in basaltic and ultramafic systems; witness the abundance of spinel peridotites among Earth's mantle rocks. The effect of pressure on spinel stability has been explored extensively (Presnall et al., 1978; Sen and Presnall, 1984; Milholland and Presnall, 1998), and has led to hypotheses that lunar spinel troctolites formed at significant pressures, 0.1 – 0.2 GPa, corresponding to the deep lunar crust and upper lunar mantle (Herzberg and Baker, 1980; Herzberg, 1983; McCallum and Schwartz, 2001; Nazarov et al., 2011), or that high pressure favors spinel formation in non-equilibrium conditions (Prissel et al., 2014).

Recognizing the difficulties of generating troctolitic magmas and of bringing deep lunar material to the surface, several groups have considered whether spinel-bearing lunar rocks could represent mixtures of basalt and ferroan anorthosite. This concept arises from the form of the liquidus surface in simple systems related to basalt, e.g. forsterite-anorthite (Fo-An), Figure 2a. In that system (and its extensions to complex natural chemical systems), compositions of mixtures of basaltic magma and anorthosite can fall in the liquidus field of spinel, or reach spinel saturation after fractionation of plagioclase or olivine. Finnila et al. (1994) showed that lunar picritic magmas (rich in normative olivine) could assimilate only small proportions of anorthosite in the crust, either by melting the anorthosite or by dissolving it. The experiments of Morgan et al. (2006), on isothermal dissolution of anorthosite in lunar picritic magma, showed that thin zones of spinel-bearing silicate melt can form at the boundary between solid anorthite and molten picritic basalt; Kohut and Nielsen (2003) found similar bands of spinel-bearing melt in reaction between anorthitic plagioclase and olivine-saturated MORB. Morgan et al. (2006) noted that lunar spinels could have formed, as in their experiments, by solution of anorthosite into picrite magma. This view is consistent with an inference that anorthosite assimilation is crucial for creating the sources of the lunar Mg-suite magmas (Warren, 1986).

This discussion, and the rest of this paper, considers only highly calcic, or anorthitic, plagioclase, such as is abundant on the Moon in its ferroan anorthosites. Alkali anorthosites, with plagioclase of An60-80, are present but rare on the Moon (Warren et al., 1983; Snyder et al., 1995). Because of their rarity, we do not consider them further.

With the detection of pink spinel anorthosites, Prissel et al. (2014) reconsidered the work of Finnila et al. (1994) and Morgan et al. (2006) in light of their new isothermal experiments and of models for the compositions and differentiation of lunar basin impact melts (Vaughan et al.,

2013; Hurwitz and Kring, 2014). Prissel's experiments, like those of Morgan et al. (2006), showed that dissolution of anorthosite into lunar picrite melt could produce selvages of spinel-bearing melts, and showed further that the Mg* (molar Mg/(Mg+Fe)) of the experimental spinels was too low to be consistent with remote sensing results; thus Prissel et al. (2014); Prissel et al. (2016a); Prissel et al. (2016b) inferred that lunar spinels were produced by assimilation of anorthosite into Mg-suite magmas, which have an appropriately high Mg* (Elardo et al., 2011; Shearer et al., 2015). Pressure may be significant in formation of spinel anorthosites, because the liquidus spinel field enlarges as pressure increases; thus spinel could form as a result of anorthosite assimilation into basaltic, not picritic, magmas at sufficiently high pressures (Prissel et al., 2014).

Enthalpy Constraints

Most of these models for the formation of spinel anorthosites and spinel troctolites invoke mixing or assimilation of anorthosite into basaltic or picritic magmas. However, assimilation requires significant energy to dissolve crystalline solids (Bowen, 1922, 1928). Because nearly all natural silicate melts are at temperatures slightly above to below their liquidi (Bowen, 1922; Yoder, 1976; Philpotts and Ague, 2009; Marsh, 2013), they can gain the heat to assimilate material only by crystallizing other phases. Most minerals have similar enthalpies of melting (per gram), so there is a near-equality between the mass of assimilant and the mass of crystallizing phases if they start at the same temperature (Morse, 1980; Kelemen, 1990). To assimilate larger amounts of material or material at low temperature requires additional heat. Finnila et al. (1994) suggested that assimilating lunar magmas had been generated at great depth, and became superliquidus in their rapid adiabatic rise toward the surface. Extra heat for

assimilation can also come from large volumes of magma, e.g. as the wall of a conduit is heated by the continual passage of hot magma (Morgan et al., 2006).

Treiman et al. (2015) reinvestigated the heat required for assimilation of anorthosite into lunar magmas and found that formation of extensive spinel-bearing rocks required more heat than would be available during simple assimilation or dissolution of anorthosite into basaltic magma. They suggested that the superliquidus melts needed for formation of abundant spinel could be impact melts (Marvin and Walker, 1985; Hess, 1994; Gross and Treiman, 2011; Demidova et al., 2017).

Methods

To understand the formation of lunar aluminate spinels, we consider the enthalpies (i.e., heats) required to produce spinel anorthosite by assimilation or dissolution of anorthite (from lunar anorthosite) into basaltic and picritic magmas. We construct phase diagrams in enthalpy-composition (ΔH^*-X) space at constant pressure, from which one can calculate the enthalpy required to produce particular assemblages of minerals and melt. For our calculations, ΔH^* is defined as the difference between the enthalpy of formation of a composition 'y' at T and P (which could include melt and/or crystals), and the enthalpy of formation of the crystalline equivalent of that composition at the reference temperature and pressure, T_0 = 25°C and P_0 = 1 bar (Ussler and Glazner, 1992),

(1) $\Delta H^*(T)y = \Delta_{fm}H(T)_y - \Delta_{fm}H(T_0)_{Solids}$,

see Appendix A.

All the calculations here are for 1-bar pressure, which (for these volatile-free systems) are considered close approximations to phase equilibria at < 1000 bars, i.e. to depths of < 2 kilometers in the Moon, e.g. (Presnall et al., 1978; Sen and Presnall, 1984). We rely primarily on

the FactSage© computational code (Bale et al., 2002), which is calibrated best for simple chemical systems, and show the results are viable using the graphical method of Ussler and Glazner (1992) and the computational MELTS code (Ghiorso and Sack, 1995).

Interpretation of enthalpy-composition phase diagrams is different from that of familiar temperature-composition diagrams (Ussler and Glazner, 1992; Glazner, 2007; Sen, 2013; Schmid-Fetzer, 2014). Temperature-composition diagrams are most useful and appropriate in circumstances where temperature is controlled externally and heat can freely enter and leave the chemical system, e.g. in an isothermal laboratory experiment, or during regional metamorphism. Enthalpy-composition diagrams are more appropriate for systems where heat cannot enter or leave (i.e., are isenthalpic) on relevant timescales, or systems where heat transfer is a controlling or rate-limiting process, e.g. in the natural cooling of magmas and impact products, and in many industrial processes. We defer discussion of the interpretation of enthalpy-composition diagrams until that for Forsterite-Anorthite has been generated.

Abbreviations for phases and chemical components used here are given in Tables 2a and 2b.

FactSage©

Equilibrium temperature-composition and enthalpy-composition phase diagrams were calculated for 1 bar pressure using the FactSage computer code (Bale et al., 2002; Bale et al., 2016), which applies the CALPHAD method (Lukas et al., 2007). Thermochemical data for FactSage are from its databases 'Silicate-Oxide Melts,' and 'FTOxid' (maintained and updated at the Center for Research in Computational Thermochemistry, École Polytechnique, Université de Montréal), for which "…the system Al_2O_3-CaO-FeO-Fe_2O_3-MgO-SiO_2 has been fully optimized from 25°C to above the liquidus temperatures at all compositions and oxygen partial pressures"

(Bale et al., 2009). These databases include non-idealities in silicate liquid solutions and in solid solutions.

There are a few significant discrepancies between the phase diagrams calculated by FactSage and those determined experimentally. FactSage calculates that both cordierite [$Mg_2Al_3(Si_5AlO_{18})$] and sapphirine [$Mg_4Al_{10}Si_2O_{13}$] are present in the sub-solidus regions in the system Forsterite-Anorthite (Fo-An), and on the liquidus surface of Forsterite-Anorthite-Silica (Fo-An-Qz); see Appendix B; neither phase has been reported in experiments in Fo-An or Fo-An-Qz. The FactSage free energies for cordierite and sapphirine appear to be too negative, so cordierite and sapphirine were excluded from the FactSage calculations here, except as specifically noted.

Of greater significance, FactSage calculates that $MgAl_2O_4$ spinel is stable over a larger range than known from experiments (see below). This difference is not significant for the geometry and interpretation of most phase diagrams here. However, the calculated increase in spinel stability is significant for the 1-bar liquidus surface in Forsterite-Anorthite-Silica (Fo-An-Qz, Appendix B), and precludes extrapolation of FactSage results to high pressures. Other small discrepancies between FactSage predictions and experimentally determined phase equilibria are not significant for our purposes.

Graphical

Phase diagrams in enthalpy-composition (ΔH^*-X) space, at 1-bar pressure, can be constructed following the method of Ussler and Glazner (1992); details are given in Appendix A. From a published T-X phase diagram, a ΔH^*-X diagram can be constructed by calculating the enthalpy of a composition (X) at a given T from knowledge of the phases present, their proportions, and their own enthalpies. This method assumes ideal mixing in both solids and

liquids; the former assumption is close to reality, as in Fe-Mg mixing in olivine (Wiser and Wood, 1991; Powell et al., 2014); the latter assumption is not strong, as will be seen below.

The graphical method is readily applied to a system's liquidus surface, where the composition of the melt phase is clearly defined. Below the liquidus, the method is more difficult because melt compositions are commonly not reported (especially in early publications). In those cases, sub-liquidus ΔH^*-X relations must be extrapolated from end-member and liquidus compositions, and are significantly uncertain. For several of the chemical systems considered here, T-X phase diagrams are not available. In those cases, we extrapolated from related systems as described below.

MELTS©

Temperature-composition phase diagrams of compositions relevant to assimilation of anorthosite by lunar picritic magmas were constructed using the MELTS computer code (Ghiorso and Sack, 1995; Ghiorso et al., 2002) as the package Rhyolite-MELTS v1.02, which is recommended for volatile free systems at low pressure (Gualda et al., 2012). MELTS was used in its equilibrium mode, i.e. at each temperature MELTS calculates the assemblage of equilibrium phases, proportions, and compositions. Input compositions were calculated as linear mass mixtures of the calculated compositions of ideal starting materials (e.g., anorthite as $CaAl_2Si_2O_8$; augite of Mg*=63 as $Ca(Mg_{0.63}Fe_{0.27})Si_2O_6$). For liquidus diagrams, MELTS was instructed only to calculate the liquidus temperature for each composition. Otherwise, MELTS was instructed to calculate the equilibrium crystallization path down-temperature, and phase appearances and disappearances were read from that output. For systems with Fe, oxygen fugacity was set in MELTS to the Fe-FeO buffer (iron-wüstite). With this oxygen fugacity, MELTS reports back small proportions of ferric iron, as Fe_2O_3, in the melt solution. At lower

oxygen fugacities such as obtain in lunar magmas (e.g., iron-fayalite-quartz or FMQ-4), MELTS typically gave similar liquidus temperatures (within 5°C), but commonly failed to converge at subliquidus temperatures.

Rhyolite-MELTS reproduces well, within 10's of °C, liquidus and sub-liquidus phase equilibria for many basaltic and picritic compositions (Balta and McSween, 2013; Arai and Maruyama, 2017), including compositions similar to those for which Rhyolite-MELTS is calibrated. However, Rhyolite-MELTS does not reproduce experimentally determined liquidus locations for some relevant composition here, especially for simplest pseudo-binary joins (see Appendix B). These problems are not unexpected, as MELTS is calibrated against experiments on natural, complex magma compositions.

Rhyolite-MELTS does calculate reasonable phase equilibria, especially liquidus surfaces, for the more complex compositions relevant to this work. For example, MELTS predicts that the Apollo 15C green glass' 1-bar liquidus is 1399°C, while experiments give 1380±10°C Elkins-Tanton et al. (2003). Similarly, MELTS predicts that the olivine-orthopyroxene-augite-plagioclase-liquid peritectic point in CMAS is at ~1215°C, while experiments place it near 1235°C (Longhi, 1987; Libourel et al., 1989). These differences are relatively minor for our purposes. As shown below, Rhyolite-MELTS yields results consistent with experiments for the liquidus surface for Fo-An-Di-FeO (Mg*=63%), and sub-liquidus equilibria between anorthite and a peridotite in that system.

Results and Interpretations of Phase Diagrams

The results of this study are phase diagrams, in temperature-composition (T-X) and enthalpy-composition (ΔH^*-X) spaces, that provide temperature and heat constraints on the formation of magnesian aluminate spinel in lunar rocks. We generated these phase diagrams

from the simplest relevant system, Mg_2SiO_4-$CaAl_2SiO_8$ (Forsterite-Anorthite, or Fo-An), by successive additions of SiO_2 (Qz), $CaMgSi_2O_6$ (Diopside), and FeO (or Qz, Di, and FeO). Rather than consider all possible chemical conditions, we focus on two realistic cases – interaction between anorthite and a picrite magma like the magnesian suite parent magma, e.g., Prissel et al. (2016a); and interaction between anorthite and a primitive lunar picrite, e.g., Morgan et al. (2006).

Result 1: The System Fo-An

T-X: The chemical system Mg_2SiO_4-$CaAl_2SiO_8$ (Fo-An) is a crucial boundary to the compositions and phase equilibria of nearly all basaltic magmas (Morse, 1980). It is the simplest system relevant to basalts in which spinel is a liquidus phase, and an approximation to one possible scenario – interaction of ferroan anorthosite with magnesian dunite or peridotite such as is expected in the upper lunar mantle (Elkins-Tanton et al., 2011). For the most part, we ignore minor non-idealities, like of Ca and Al solid solutions in forsterite olivine, of Mg solution in anorthite plagioclase, and of spinel non-stoichiometry.

The temperature-composition (T-X) phase diagram for Fo-An (Fig. 2a) is known from laboratory experiments (Andersen, 1915; Osborn and Tait, 1952; Irvine, 1974). It can also be calculated from thermochemical models of the phases and melt solutions, as in Figure 2b by FactSage.[1] These supersolidus portions of these figures are slightly different, but effectively identical within the uncertainties of phase boundary locations and thermochemical parameters. The most significant difference between the supersolidus portions is in the extents of the Sp stability fields; the FactSage calculated diagram shows spinel to be stable in slightly greater

[1] The Rhyolite-MELTS computer code does not replicate phase equilibria in Fo-An adequately, see Appendix B.

composition and temperature ranges than do laboratory experiments. In the sub-solidus, the diagrams appear different in that the FactSage version (Fig. 2b) shows subsolidus Opx and Sp. The presence of Opx and Sp in the diagrams must reflect non-idealities in FactSage's calculated compositions of Ol and An. By the phase rule, Opx and Sp can not be present if Ol and An have ideal stoichiometric compositions. From this argument, the proportions of Opx and Sp must be vanishingly small.

ΔH*-X: Figures 2c and 2d show enthalpy-composition (ΔH*-X) diagrams for Fo-An. Figure 2c is constructed from Figure 2a and thermochemical data by the method of Ussler and Glazner (1992), see Appendix A. Figure 2d is the enthalpy-composition (ΔH*-X) diagram generated from the FactSage code and database. These two diagrams are identical in topology, i.e. the identities of the fields and their configurations – both methods place invariant and univariant points at nearly identical compositions, enthalpies, and temperatures. However, the liquidus curves and high-temperature isotherm lines are significantly different. In Figure 2c, both types of lines are straight because the Ussler and Glazner (1992) method assumes that the silicate melt is an ideal solution; these lines are curved in Figure 2d because FactSage accounts for the melt solution non-idealities.

Interpretation 1: The System Forsterite - Anorthite.

Interpretation of the T-X diagram for Fo-An (Figs. 2a, 2b) is straightforward and familiar, e.g. Chapter 9 of Morse (1980). Its crucial features are that: forsterite and anorthite each melts congruently; melts of some intermediate compositions crystallize spinel first as they cool; and that spinel is not stable below the system's solidus. If one ignores spinel, the system is similar to a typical binary eutectic like forsterite-diopside (Bowen, 1914; Osborn and Tait, 1952); the presence of liquidus spinel interrupts that simplicity by adding fields of L + Sp, L + Sp + Ol, and

L + Sp + Pl. Also different, in place of a eutectic point, is a peritectic point representing the reaction L + Sp = Ol + Pl.

ΔH*-X diagrams are uncommon in petrologic applications, and so require explanation (Yoder, 1975; Ussler and Glazner, 1992; Glazner, 2007). First, Figures 2c & d show that isotherms are not isenthalpic. For instance, the 1500°C isotherm in Figure 2d spans ΔH* from 1.65 kJ/gm (pure Pl) to 2.65 kJ/gm (on the Ol liquidus surface). Conversely, isenthalpic lines are not isothermal. For example, the blue line on Figure 2a is at ΔH* = 1.8 kJ/gm (from Fig. 2c), and is clearly not isothermal. The primary reason that isotherms are not at constant enthalpy is heat of crystallization – significant energy is required turn a crystalline solid to a melt, even if that melt is part of a complex melt solution. Somewhat less important here is non-ideality in the melt solution, which can be seen in the curvatures of isotherms in the L (melt-only) field in Figure 2d.

Another important distinction is that the peritectic or eutectic invariant points, like the L + Sp = Ol + Pl point on Figures 2a & b, appear as fields in ΔH*-X diagrams (e.g., L + Sp + Ol + Pl, in Figures 2c & d). As a system crystallizes at such a peritectic or eutectic, the temperature remains constant, but significant heat of crystallization must leave the system for crystallization to proceed (e.g., as L + Sp => Ol + Pl).

Finally, the ΔH*-X diagram provides a basic framework to understand assimilation. Assimilation can be modeled as an isenthalpic process; mixing and dissolution of solids into a melt involves no heat exchange with an external reservoir. Thus, the total enthalpy of the system is the same before and after mixing and dissolution. Note especially that temperature is not conserved, because energy can be transformed from thermal to chemical, in the form of different atomic bonding in the crystalline and molten states. For example, consider mixtures of solid forsterite olivine at 1550°C and solid anorthite plagioclase at 1550°C (the green line in Fig. 2c).

Equilibrium mixtures along that line are at lower temperatures than at either end, because the mixtures are partially molten (i.e., thermal energy is converted to configurational energy). Some such mixtures will even cool to 1293°C, the peritectic temperature (L + Sp + Ol + Pl).

Spinel Formation: The ΔH*-X diagrams provide constraints on assimilation as a process in formation of 'spinel anorthosites,' i.e., fields on Figures 2c & d that have spinel and/or anorthite but not olivine. On the ΔH*-X diagrams, products of assimilation of anorthite into any melt composition fall on a straight line between the points with the composition and ΔH* of each component (because both elements and enthalpy are conserved). To produce 'spinel anorthosite,' such a line must cross the L+Sp or L+Sp+An fields; 'spinel anorthosite' would then arise by mixing of compositions at the line ends to give an X and ΔH* in those fields, and then quenching to prevent formation of significant olivine (via the L+Sp=>Ol+An peritectic). Assimilation of anorthite into an arbitrary melt, for instance the 'am' point (green) in Figure 2e (1900°C, 40% An), can yield 'spinel anorthosite' directly or on realistic cooling for anorthite with low ΔH*, and thus low T; any mixture of the 'am' and anorthite to the right of the green dashed line in Figure 2e could fall in a 'spinel anorthosite' field (pink) or pass into one while cooling.

However, natural magmas do not have arbitrary compositions and temperatures (i.e., enthalpy contents). With few exceptions (Sparks et al., 1977; Hess, 1994), magmas are restricted to temperatures below or slightly above their liquidi (Bowen, 1922; Yoder, 1976), i.e. superliquidus magmas are rare. Thus, the equivalents in Fo-An of natural magmas must fall near or at lower ΔH* than the liquidus surfaces. As in Figure 2, three cases of such melts are possible: on the olivine liquidus, on the spinel liquidus, and on the plagioclase liquidus.

First, consider a melt in Fo-An on the olivine liquidus at 70% Fo and ~1670°C, the violet point 'im' on Figure 2e. For such melts to assimilate anorthite and yield 'spinel anorthosite', the

anorthite must have $\Delta H^* > 1.4$ kJ/gm ($T > \sim 1300°C$), i.e. to the right of the violet line in the Figure. Otherwise, the assimilated mixture would contain olivine and thus not appear in reflectance spectra as spinel anorthosite. This result is applicable to any composition that has olivine on its liquidus.

For a second example, consider a melt in the Fo-An system with spinel on the liquidus. That melt could yield a spinel anorthosite directly; similarly, if that melt were to assimilate some An at any temperature, the mixture would be in a spinel anorthosite field or pass through one on cooling, and thus yield a spinel anorthosite rock. However, the path to generating a magma with spinel on its liquidus is not clear – melts of a typical peridotite mantle (i.e., from a fundamentally chondritic planetary body) would yield melts on the olivine liquidus. Melting of a troctolite rock (plagioclase + olivine) could yield a melt on the spinel liquidus, but the origins of troctolites themselves and how they could be melted are not clear (James and Hedenquist, 1978; Hess, 1994; Ariskin, 2007; Prissel and Gross, 2018).

Third, a magma on the anorthite liquidus could yield spinel anorthosite material as it cools, with or without assimilation of anorthite. Again, it is not clear how such melt could be formed, except perhaps by melting of anorthosite plus a small proportion of dunite or peridotite. This scenario could occur on small scale by impact melting of a layered basaltic intrusion that had layers of anorthosite and dunite, perhaps like the Stillwater intrusion (McCallum, 1996). Or, for instance, it could represent a large scale impact mixing and melting of crustal ferroan anorthosite with magnesian peridotite of the Moon's upper mantle, vis Figure 6 of Treiman et al. (2010).

To summarize, melts on the olivine liquidus surface in Fo-An cannot assimilate anorthite and yield spinel anorthosite unless the anorthite is already very hot, above ~1300°C. Conversely,

spinel anorthosite cannot be generated from cold anorthite assimilant unless the assimilating magma is very hot and/or is already relatively rich in An component.

Result 2: Peridotite-Anorthosite in the System Fo-An-Di-Qz

To extend our results toward realistic lunar compositions, we first consider Fo-An with additional SiO_2, the system Fo-An-Qz, and then with added diopside component, $CaMgSi_2O_6$, for the system Fo-An-Di-Qz. In these systems, we focus on joins between anorthite and peridotite compositions such that the joins include projections of the Apollo 14 B green glass composition. We chose the A14B composition because it is among the most picritic (i.e., olivine-normative) and magnesian of known lunar magmas (see Appendix C). In both systems, these joins pass close to proposed compositions of a Mg-suite Parental Magma composition, MgSPM (Longhi et al., 2010; Prissel et al., 2016a), allowing us to consider both magma compositions with a single diagram. Phase equilibria along these joins are similar, so we relegate the diagrams and discussion of Fo-An-Qz to Appendix D.

The larger chemical system, Fo-An-Di-Qz, includes all the major minerals in common basalts, and so should approximate equilibria in highly magnesian natural systems (e.g., the Mg-Suite parent magma composition, Table 1). Figures 3a and 3b show the ternary liquidus surface of the Qz-absent subsystem thereof (Fo-An-Di), and the projected compositions of the Apollo 14 B green glass, A14B' (Delano, 1986; Elkins-Tanton et al., 2003), and estimated Mg-Suite parent magma, MgSPM' (Longhi et al., 2010; Prissel et al., 2016a). As above, we selected a join between anorthite and a diopside-bearing (Fe-free) peridotite composition, Perid14B' (Table 1), in blue on Figures 3a & 3b. The join includes the A14B' composition, and passes close to the MgSPM' composition.

There are limited experimental data along, or closely relevant to, the join Perid14B'–An, so the experimental T-X and graphical ΔH*-X diagrams (Figs. 3c,e) required considerable estimation and extrapolation from published data (Bowen, 1914; Kushiro et al., 1972; Pan and Longhi, 1990) and from phase equilibria calculated via Rhyolite-MELTS. The liquidus temperature of Perid14B' is taken as 1730°C, interpolated between values of ~1740°C from experiments in Fo-Di-Qz (Bowen, 1914), and a value of 1727°C from the Rhyolite-Melts v1.02 model. This temperature is 50°C lower than the liquidus of Perid14B' (Fig. 3), and we take that difference as the effect of the added Di component in the liquid. That reduction in temperature is extrapolated linearly, implicitly assuming ideal solution in the melt (Ussler and Glazner, 1992) across the join to anorthite; for example, a composition of 80% Perid14B' and 20% Anorthite is assigned a liquidus temperature 40°C lower than its projection (from Di) into the Fo-An-Qz system (Osborn and Tait, 1952). The sub-liquidus portions of the T-X diagram for Perid14B'-An, for compositions <~50% anorthite, are as calculated with the Rhyolite-MELTS v1.02 code, which gives results that are consistent with the limited available experimental data, and otherwise appear reasonable. The sub-liquidus portions of the diagram for compositions richer in anorthite component are extrapolated from graphical constructions of simpler systems like Fo-An system (Fig. 3b), and from other joins for which more data are available (Treiman et al., 2015).

The phase diagrams calculated with FactSage (Figs. 3b,d) are very similar to those from (and extrapolated from) laboratory experiments, except that the spinel liquidus field is again enlarged somewhat (see also Figs. 2a,b, B2). The spinel fields here do not intrude so much into the sub-liquidus regions as they do in Fo-An-Qz (see Appendix B).

Interpretation 2: Peridotite-Anorthosite in the System Fo-An-Di-Qz.

Temperature-composition (T-X) diagrams for the join Perid14B'-An (Figs. 3c, d) are similar to those for the system An-Fo (Figures 2a, b), especially for An-rich compositions relevant to spinel formation. Both versions of the T-X diagrams for Perid14B'-An show a field of liquidus spinel, fields of L+Sp+An and L+Sp+Ol, and a peritectic for L+Sp = An+Ol. These fields and peritectic in Perid14B'-An are at lower temperatures than in Fo-An, which reflects the presence of both Di and Qz components as diluents. The An-rich ends of the diagrams are similar to those in Fo-An, with no additional fields or changes in geometry. The An-poor ends of the phase diagrams are far more complex than in Fo-An, as pyroxenes (low- and high-Ca) enter and leave the crystallization sequence. However, none of these complexities of pyroxene crystallization (Appendix B) affect equilibria involving spinel.

As with the T-X diagrams, the ΔH^*-X diagram for Perid14B'-An (Fig. 3e) is similar to those for Fo-An, with differences in the low-temperature and An-poor relations and in the lower overall ΔH^* (again, representing the lower temperatures from the diluent effects of Di and Qz components). As such the interpretation of these diagrams for formation of spinel and 'spinel anorthosites' are similar to those for the system Fo-An. In the larger systems, melts at superliquidus temperatures can yield 'spinel anorthosite' (i.e. fall in a pink phase field) by assimilation of anorthite, cold or hot. Melts on the spinel- and plagioclase-liquidus surfaces also can yield 'spinel anorthosite,' although generation of such melts is (as above) problematic. Melts that lie on the olivine liquidus surface (e.g., A14B') cannot assimilate anorthite and yield 'spinel anorthosite' unless the anorthite is already very hot, above ~1300°C.

Result 3: Peridotite-Anorthosite with Iron, in the System Fo-An-Di-Qz-FeO

The results above, for a model iron-free A14B picrite and peridotite, are adequate models for the calculated Mg-suite Parent Magma (MgSPM) at Mg*=86% (Prissel et al., 2016a), which has not been found directly but only inferred from mineral compositions of lunar Mg-Suite plutonic rocks. However, most lunar magmas are much more ferroan, and one needs to explicitly consider the effects of iron on their phase equilibria. Here, we focus on the Apollo 14B green glass because it is among the most magnesian of known lunar magmas, at Mg*=63% (Elkins et al., 2000). Most other lunar basaltic magmas have Mg* between 40% and 50% (Papike et al., 1998), so that assimilation of anorthosite into them should be less likely to yield spinel than assimilation into the A14B green glass (see below).

To understand phase equilibria relevant to the A14B green glass at 1 bar, we calculated liquidus and sub-liquidus phase equilibria in the system Forsterite-Anorthite-Diopside-FeO (Mg*=63%) and on the join Perid14B-Anorthite (Table 1; Figure 4) using the both the FactSage and Rhyolite-MELTS software packages. Both sets of computed results are consistent with the limited experimental data relevant to the Apollo 14 B green glass composition and the A14B peridotite (Figure 4). There are no published data on low-pressure liquidus and sub-liquidus phase equilibria for the A14B composition, and only limited data on bounding joins at Mg* relevant to A14B, specifically on the olivine-augite join (Roedder, 1965; Huebner and Turnock, 1980), and the olivine-anorthite (Walker et al., 1973; Lipin, 1978). The available liquidus data on the A14B composition are for high-pressure (> 1.3 GPa) conditions (Elkins et al., 2000), related to its origin in the lunar mantle.

The results of the MELTS and FactSage models for Forsterite-Anorthite-Diopside-FeO (Mg*=63%) and Perid14B-Anorthite are similar, but with differences that highlight the

inconsistencies between the computational models. We note that this Fe-bearing system is within (or close to) the compositional space of natural magmas for which MELTS is calibrated (Ghiorso and Sack, 1995; Ghiorso et al., 2002; Gualda et al., 2012); the FactSage model was calibrated primarily for binary and ternary chemical systems (Saxena, 2010), so it is less certain for more complex compositions.

The most significant difference between the models, as observed for the system Fo-An (see Appendix B), is that MELTS calculates significantly smaller fields of spinel presence than does FactSage. This difference persists in to the complex system here: FactSage calculates that the system Perid14B-Anorthite has a field of liquidus spinel (Fig. 4c), while MELTS would have no field of liquidus spinel (Fig. 4b). In fact, the MELTS model replicates experimental results for spinel-melt equilibria along the olivine-anorthite join adequately (Fig. 4a). Another significant difference, although of limited importance here, is that FactSage appears to overestimate liquidus temperatures along the olivine-diopside join for Mg*=63, see Figures 4 a-d. The cause of that discrepancy is not clear.

Interpretation 3: Effects of FeO on phase equilibria.

The effects of adding FeO to the system Fo-An-Di are clear and expected, see Figures 3a,b compared to Figure 4a. The addition of iron lowers liquidus temperatures across the diagrams, and thereby expands the liquidus field (and sub-liquidus fields) of anorthite, which is unaffected by the FeO. The field of liquidus olivine contracts significantly, as expected from relations in the simple system Mg_2SiO_4-Fe_2SiO_4 (Bowen and Schairer, 1935). The field of liquidus augite expands significantly at the expense of the olivine field, because liquidus temperatures in Mg-rich portions of $CaMgSi_2O_6$-$CaFeSi_2O_6$ are nearly isothermal (Fig. 3e of Huebner and Turnock (1980)).

Of most significance here, the field of liquidus spinel shrinks significantly with addition of FeO, compare Figures 3a-e and 4a-d. The results here are consistent with experimental determinations by: Osborn and Tait (1952) for Mg*=100, Lipin (1978) for Mg*=59, Walker et al. (1973) for Mg*=30, and Schairer (1942) for Mg*=0. The field of spinel stability shrinks relative to that of anorthite because, of course, spinel does take significant FeO in solid solution and anorthite does not. The spinel liquidus field also shrinks relative to that of olivine, because Mg is partitioned preferentially into olivine relative to spinel; the partition coefficient for Mg/Fe between olivine and spinel greater than 1, i.e. $^{(Mg/Fe)}D_{(ol/sp)} \geq 1.5$ (Prissel et al., 2016a). Thus, the spinel liquidus field shrinks relative to those of both olivine and anorthite with increasing Fe content, i.e. decreasing Mg*.

In enthalpy-composition space, phase relations on the Perid14B-Anorthite join (Figure 4d) are similar to those on the Fe-free join Perid14B'-Anorthite (Figure 3e), with nearly identical geometries but lower enthalpies. Clearly it takes less enthalpy (i.e., lower temperature) to melt Fe-bearing peridotite and picrites (e.g., A14B) than their Fe-free equivalents (e.g., A14B'). The An-rich ends of the joins are similar, with the spinel-bearing fields bent to lower T and lower An content in the Fe-bearing system (Fig. 4).

Implications & Discussion

Spinel Formation via Assimilation

A leading hypothesis for the formation of lunar spinel, and specifically spinel anorthosite, is by assimilation of anorthite plagioclase from lunar highlands rocks into basaltic or picritic magmas (Finnila et al., 1994; Morgan et al., 2006; Prissel et al., 2014; Prissel et al., 2016a; Prissel et al., 2016b). However, summarizing the results above, simple assimilation of highlands

crust anorthosite into basaltic or picritic magma cannot yield spinel anorthosite. Consider, for example, an attempt to form spinel anorthosite by assimilation of anorthite (from ferroan anorthosite) into a model (Fe-free) Apollo 14B green glass picrite (A14B') at its liquidus (Figure 3). On Figure 3e, that would appear on the A14B' line at ΔH^* of ~2.4 kJ/gm, or at T~1600°C. Because enthalpy is conserved during assimilation, the task is to find straight lines from that point on Figure 3e that cross the pink fields; materials quenched from the pink fields would appear (in VNIR remote sensing) as spinel anorthosites. All such possible straight lines involve anorthositic compositions at high ΔH^*, at least 1.2 kJ/gm (for nearly pure anorthosite, the lowermost right corner of the pink fields), i.e., at T > ~1290°C. Essentially identical results obtain for the Fe-bearing system, except that the fields that could produce spinel anorthosite are smaller still (Fig. 4d). In other words, spinel anorthosite can be produced by assimilation of anorthosite into picrite (A14B or A14B') only if the anorthosite is very hot, >~1300°C. Assimilation of cold anorthosite into picritic magma cannot produce spinel anorthosite – its products will always contain olivine.

If generation of spinel anorthosite requires a hot anorthosite precursor, how can that precursor be heated? Two mechanisms have been suggested: heating by large volumes of picritic melt (Morgan et al., 2006; Prissel et al., 2014), and pre-heating by planetary scale tidal deformation (Meyer et al., 2010; Elkins-Tanton et al., 2011; Tian et al., 2017).

In the first mechanism, anorthosite can become hot enough to generate spinel with heat from the assimilating picritic magma, for instance in the walls of a dike that traversed anorthosite (Morgan et al., 2006). To examine one specific scenario, one that could produce significant masses of spinel anorthosite, consider thermal equilibration but not chemical mixing of equal masses of A14B' picrite at its liquidus, and pure anorthosite at 25°C (Fig. 3e). The ΔH^* of the

mix would be ~1.25 kJ/gm = (2.5+0)/2 kJ/gm, which would be consistent with production of a small proportion of spinel in the anorthosite. If, however, there was any chemical exchange between the anorthosite and the picrite, e.g., Fig. 5c of Prissel et al. (2014), olivine would be formed (Fig. 3e). Thus, to make abundant spinel anorthosite, the heat from another pulse of magma must be added to the anorthosite.

This scenario presents two significant problems. First, the idea of static thermal equilibration is far from the actual conditions of heat transfer in a dike – a significantly larger mass of picrite magma must pass through a dike to heat its wall rock so much. Second is that some exposures of spinel anorthosite are not associated with obvious signs of basaltic or picritic magmatism, which ought to be present if this simple scenario has any validity. Most recognized exposures of spinel anorthosite are reasonably close to basaltic igneous rocks, including: crater-filling flows like at Moscoviense and at Thomson (Pieters et al., 2011; Pieters et al., 2014); massifs within basins like Teneriffe Montes (Pieters et al., 2014); and floor-fractured craters like Dalton, which are inferred to overlie intrusive bodies of basaltic magma (Pieters et al., 2014) . In other sites, association with basaltic magma is less clear, like the central peaks of Theophilus crater, which is adjacent to the basalt-filled Nectaris basin (Dhingra et al., 2011; Lal et al., 2012; Pieters et al., 2014). And significantly, there are several sites with spinel anorthosite that are not associated with obvious basaltic magmatism, like Geminus crater (Pieters et al., 2014), Tycho crater (Kaur et al., 2012), and the craters Golitsyn, Copernicus, and Goodacre (Sun et al., 2017). While several mechanisms for spinel formation are likely to have operated on the Moon, the remote sensing data seem inconsistent with picrite assimilation as the single mechanism.

On the other hand, tidal flexure can heat a planetary body significantly, with the best examples being Jupiter's Moons Io and Europa (Peale et al., 1979; Sotin et al., 2009). Tidal

heating is not important now for the Moon, but would have been important in its early history because the Moon was closer to the Earth. Late in the Moon's magma ocean stage, it would have had a solid anorthosite crust overlying molten silicate, and the anorthosite would have been heated by tidal flexure, even to near its melting point (Meyer et al., 2010; Elkins-Tanton et al., 2011; Tian et al., 2017). Under those conditions, intrusions of picritic magma would have inevitably produced spinel anorthosites and troctolites. If this scenario had prevailed, lunar spinel anorthosites should show evidence for high pressure (some do and some do not), and should be ancient, with ages > 4.3 Ga (Elkins-Tanton et al., 2011).

There are nearly no age determinations for lunar spinel-bearing rocks (i.e. troctolites), in part because of their small masses (Shearer et al., 2015). The only radiometric age appears to be for the spinel troctolite breccia clast 73215,170 (Blanchard et al., 1977; James and Hedenquist, 1978), which gave an Ar-Ar age of 4.46 Ga for the highest-temperature gas release (Jessberger, 1979). Unfortunately, this age has not been peer-reviewed nor confirmed independently. Broadly, the Apollo spinel troctolites are expected to be pre-Imbrian, i.e. > 3.91 Ga (Snape et al., 2017), and could reasonably have ages in the 4.34-4.37 Ga range, as is typical of highlands samples and lunar zircons (Borg et al., 2015; Crow et al., 2017).

Superliquidus Impact Melts

Given the strict constraints that enthalpy places on spinel formation by anorthosite assimilation, it is sensible to consider conditions where enthalpy (heat) is abundant. The most obvious of these is in hypervelocity impacts, when an asteroidal or cometary body strikes the Moon's surface at speeds of kilometers per second. The Moon's surface is pocked by craters produced in such impact, and products of hypervelocity impacts are recognized across the lunar surface and in lunar samples.

Hypervelocity impacts can produce significant volumes of superliquidus melt, i.e. melts (and consequent glasses and rocks) that originated significantly above their equilibrium liquidus temperatures. Evidence for supherliquidus impact melts comes from many directions: theory, lunar samples themselves, lunar geomorphology, and terrestrial analogies. From theoretical models of impact cratering, it is clear that significant quantities of materials can be heated well above their liquidi, and even to extensive vaporization (O'Keefe and Ahrens, 1975; O'Keefe and Ahrens, 1977; Melosh, 1989; Johnson et al., 2015). Impact craters and their ejecta cover most of the Moon's surface, especially the highlands where anorthositic material is common; thus, one should expect that impact melts, superliquidus or not, would be abundant on the Moon.

Many lunar samples provide evidence for superliquidus impact melts, at least at the scales of the samples and their constituents. The mere existence of lunar troctolites and troctolitic compositions (many bearing spinel, Figs. 1a-c) suggests the existence of superliquidus melts (Hess, 1994): "Alternatively, the parental magmas to lunar troctolites may be impact melts of the anorthositic crust and the Mg-rich dunitic cumulates of the magma ocean" (see Treiman et al., 2010). Or, "Liquidus temperature of the 73215,170 melt should have been ~1450°C …, and the other fine-grained spinel troctolites have liquidus temperatures >1300°C …; temperatures as high as these would be unlikely for endogenous magmas, but much more likely for impact melts of preexisting rocks" (James and Hedenquist, 1978). Many lunar impact melt breccias contain rounded fragments of crystalline rock, and the rounding is inferred to represent resorption or dissolution of the rock into surrounding melt, Figure 1d (Simonds, 1975; Ryder and Spudis, 1987; Cohen et al., 2004). More directly but at a smaller scale, lunar regolith contains common fragments of crystal-free glass with compositions like those of bulk lunar rocks, from pure anorthosite through peridotite, e.g., Fig. 8 of Korotev et al. (2010). These glass fragments are

prima facie evidence for the existence of superliquidus impact melts, e.g. Fig. 1c of Bence and Grove (1978). Some impact glasses have compositions that could have become spinel anorthosites, for instances: the HASP glasses of Naney et al. (1976) and Korotev et al. (2010), the gabbroic anorthosite glasses of Ridley et al. (1973) and Naney et al. (1976), and lunar meteorite glass B1 of Ryder and Ostertag (1983). Crystalline fragments of similar composition could also have been superliquidus impact melts, but which had time to crystallize, e.g., Shervais et al. (1988).

The geomorphology of pools and flows of impact melt, imaged at high resolution by the Lunar Reconnaissance Orbiter Camera, provides additional indirect evidence for superliquidus melts. Many impact melt masses show evidence that they were very fluid, which is inferred to imply superheat (Bray et al., 2010; Denevi et al., 2012; Öhman and Kring, 2012; Stopar et al., 2014).

Finally, products of terrestrial impacts may be taken as analogs for lunar products, and can be studied in their geologic settings and environments. Many impact melts on Earth show strong evidence for superheat. The original evidence for superheat came from glasses at the classic Ries crater, Germany (El Goresy, 1965; Hörz, 1965), and that inference has been confirmed at many other impact sites (Carstens, 1975; Grieve et al., 1977; Dressler, 1984; Riller et al., 2010; Pittarello and Koeberl, 2013; Timms et al., 2017; Walton et al., 2017). At a larger scale, there is evidence that impact melt pools contained significant quantities of superliquidus melts (Zieg and Marsh, 2005; Marsh, 2013).

Spinel Formation in Impact Melts

Having established that superliquidus impact melts were present across the Moon, it remains only to indicate which compositions could yield spinel anorthosites, and what thermal

histories would be required. Simply, spinel anorthosite could potentially form from any composition and temperature (or ΔH* content) that could cool down through a field of Sp+L, or Sp+An+L (Fig. 3c-e, Fig. 4c-d). To first order, a superliquidus mixture of anorthosite and picrite (or picritic basalt, or olivine, or dunite) with more than 50% anorthosite has the potential to yield spinel anorthosite. Any such superliquidus composition will pass through either the Sp+L or Sp+An+L fields on cooling. However, slow or extended cooling of such compositions would allow the spinel to react out via the Sp + L => Ol + Pl peritectic, and yield a rock either with no spinel, or one with detectable olivine; neither would appear as a spinel anorthosite. So, rapid cooling is also required, which would be a reasonable thermal history for an impact melt.

One might reasonably ask how much spinel could be produced from such a superliquidus impact melt, and whether that would be detectable by VNIR remote sensing. There are limited data on the abundances of spinel in natural or synthetic melts in basalt-relevant systems (Figs. 3, 4), but abundances over 10% (volume) seem unlikely (Gross et al., 2014). Iron in $(Mg,Fe)Al_2O_4$ spinel has a very strong, distinctive absorption near 2-μm (Cloutis et al., 2004; Pieters et al., 2011; Cheek and Pieters, 2014; Gross et al., 2014; Jackson et al., 2014), and would be detectable by instruments like the M^3 on Chandraya'an (in the absence of interfering absorptions) at levels of only a few percent (Gross et al., 2014; Jackson et al., 2014). Several lunar samples contain far more than 10% spinel (e.g., Figure 1), and have been inferred to be products of spinel accumulation, e.g., by crystal settling (Prinz et al., 1973; Marvin and Walker, 1985). Other spinel-rich samples, especially those with small grains (e.g., Fig. 1c) could represent products of boundary-layer diffusion (e.g., Fig. 1f) as demonstrated by Kohut and Nielsen (2003), Morgan et al. (2006), and Prissel et al. (2014).

This is a preprint, the final version is subject to change, of the American Mineralogist (MSA)
Cite as Authors (Year) Title. American Mineralogist, in press.
DOI: https://doi.org/10.2138/am-2019-6652

Summary

Spinel is an uncommon mineral in rocks of the lunar highlands, but can be an important indicator of physical and chemical conditions (i.e., pressure and/or chemical composition) and thermal history. Many occurrences of lunar spinel have been ascribed to assimilation, at low pressure, of highlands anorthosite into olivine-rich basaltic (i.e., picritic) magmas. However, spinel production by assimilation requires additional heat (i.e., enthalpy) beyond that available in hot magma plus cold rock.

The additional heat for spinel formation could come from several processes: pre-heating the rock by repeated (or continuous) passage of magma, pre-heating by global tidal flexure, or superliquidus impact melts. None of these processes can be excluded for the Moon, but superliquidus impact melts seem most likely based on the ubiquity of impact craters, the abundance of impact-metamorphosed lunar rocks, and the common presence in lunar regolith of impact glasses (quenched superliquidus impact melts) of appropriate compositions.

Preservation of spinel in compositions in the "basalt tetrahedron", Fo-An-Di-Qz at any Mg*, requires rapid cooling so that the spinel does not react with melt to form olivine + plagioclase. This is consistent with origins from impact melts, is possibly consistent with pre-heating of anorthosite by magma, and is probably inconsistent with global tidal flexure of anorthositic crust. However, spinel can be preserved in rock compositions enriched in Al_2O_3 compared to the "basalt tetrahedron." Among lunar rocks, such aluminous compositions are found only in a few spinel troctolites, which are inferred to form by accumulation of spinel crystals in a melt (Prinz et al., 1973; Marvin et al., 1989; Gross and Treiman, 2011).

High pressure does stabilize spinel in basaltic and peridotitic compositions; we have not evaluated the heat requirements for spinel formation at high pressures. But near the lunar surface,

the most likely process of spinel formation is rapid crystallization of impact melts of anorthosite+picrite or anorthosite+peridotite compositions. In this model, the presence of spinel anorthosite in the walls and central peaks of impact craters signals only rapid cooling and partial crystallization of melts produced in the impact, and not uplift of deep material to the Moon's surface.

Acknowledgments

Supported in part by NASA grants NNX13AF54G to Dr. Juliane Gross (Rutgers University NJ), NNX12AH64G to AHT, and the SSERVI node at the Lunar and Planetary Institute (D. Kring, PI). We appreciate assistance and access to images from J. Gross, and discussions with T. Prissel. We acknowledge early assistance with the FactSage code from P. Hudon, J.-P. Harvey, and I.-H. Jung. We are grateful for careful reviews by Marc Norman, Becky Lange, and Steven Simon. LPI-USRA Contribution #20xx.

REFERENCES

Andersen, O. (1915) The system anorthite-forsterite-silica. American Journal of Science, 232, 407-454.

Arai, T., and Maruyama, S. (2017) Formation of anorthosite on the Moon through magma ocean fractional crystallization. Geoscience Frontiers, 8(2), 299-308.

Ariskin, A. (2007) Parental magmas of lunar troctolites: Genetic problems and estimated original compositions. Geochemistry International, 45(5), 413-427.

Baker, M.B., and Herzberg, C.T. (1980) Spinel cataclasites in 15445 and 72435 - Petrology and criteria for equilibrium. Lunar and Planetary Science Conference Proceedings, 11, p. 535-553.

Bale, C., Bélisle, E., Chartrand, P., Decterov, S., Eriksson, G., Gheribi, A., Hack, K., Jung, I.-H., Kang, Y.-B., and Melançon, J. (2016) FactSage thermochemical software and databases, 2010–2016. Calphad, 54, 35-53.

Bale, C., Bélisle, E., Chartrand, P., Decterov, S., Eriksson, G., Hack, K., Jung, I.-H., Kang, Y.-B., Melançon, J., and Pelton, A. (2009) FactSage thermochemical software and databases—recent developments. Calphad, 33(2), 295-311.

Bale, C., Chartrand, P., Degterov, S., Eriksson, G., Hack, K., Mahfoud, R.B., Melançon, J., Pelton, A., and Petersen, S. (2002) FactSage thermochemical software and databases. Calphad, 26(2), 189-228.

Balta, J.B., and McSween, H.Y. (2013) Application of the MELTS algorithm to Martian compositions and implications for magma crystallization. Journal of Geophysical Research: Planets, 118(12), 2502-2519.

Bence, A., and Grove, T.L. (1978) The Luna 24 highland component. In J.J. Papike, and R.B. Merrill, Eds. Mare Crisium: The view from Luna 24, p. 429-444. Pergamon, Houston Texas.

Blanchard, D., Jacobs, J., and Brannon, J. (1977) Chemistry of ANT-suite and felsite clasts from consortium breccia 73215 and of gabbroic anorthosite 79215. Lunar and Planetary Science Conference Proceedings, 8, p. 2507-2524.

Borg, L.E., Gaffney, A.M., and Shearer, C.K. (2015) A review of lunar chronology revealing a preponderance of 4.34–4.37 Ga ages. Meteoritics & Planetary Science, 50(4), 715-732.

Bowen, N.L. (1914) The ternary system: Diopside-forsterite-silica. American Journal of Science, 225, 207-264.

-. (1922) The behavior of inclusions in igneous magmas. The Journal of Geology, 30(6), 513-570.

-. (1928) The Evolution of the Igneous Rocks. Princeton University Press, Princeton, New Jersey.

Bowen, N.L., and Schairer, J.F. (1935) The system MgO-FeO-SiO_2. American Journal of Science(170), 151-217.

Bray, V.J., Tornabene, L.L., Keszthelyi, L.P., McEwen, A.S., Hawke, B.R., Giguere, T.A., Kattenhorn, S.A., Garry, W.B., Rizk, B., and Caudill, C. (2010) New insight into lunar impact melt mobility from the LRO camera. Geophysical Research Letters, 37(21).

Carstens, H. (1975) Thermal history of impact melt rocks in the Fennoscandian Shield. Contributions to Mineralogy and Petrology, 50(2), 145-155.

Cheek, L.C., and Pieters, C.M. (2014) Reflectance spectroscopy of plagioclase-dominated mineral mixtures: Implications for characterizing lunar anorthosites remotely. American Mineralogist, 99(10), 1871-1892.

Christophe-Michel-Levy, M., Levy, C., Caye, R., and Pierrot, R. (1972) The magnesian spinel-bearing rocks from the Fra Mauro formation. Lunar and Planetary Science Conference, 3, p. 887-894.

Cloutis, E.A., Sunshine, J., and Morris, R. (2004) Spectral reflectance‐compositional properties of spinels and chromites: Implications for planetary remote sensing and geothermometry. Meteoritics & Planetary Science, 39(4), 545-565.

Cohen, B.A., James, O.B., Taylor, L.A., Nazarov, M.A., and Barsukova, L.D. (2004) Lunar highland meteorite Dhofar 026 and Apollo sample 15418: Two strongly shocked, partially melted, granulitic breccias. Meteoritics & Planetary Science, 39(9), 1419-1447.

Crow, C.A., McKeegan, K.D., and Moser, D.E. (2017) Coordinated U–Pb geochronology, trace element, Ti-in-zircon thermometry and microstructural analysis of Apollo zircons. Geochimica et Cosmochimica Acta, 202, 264-284.

Daubar, I.J., Kring, D.A., Swindle, T.D., and Jull, A. (2002) Northwest Africa 482: A crystalline impact‐melt breccia from the lunar highlands. Meteoritics & Planetary Science, 37(12), 1797-1813.

Delano, J.W. (1977) Experimental melting relations of 63545, 76015, and 76055. Lunar and Planetary Science Conference Proceedings, 8, p. 2097-2123.

-. (1986) Pristine lunar glasses: Criteria, data, and implications. Journal of Geophysical Research: Solid Earth, 91(B4), 201-213.

Demidova, S., Nazarov, M., Ryazantsev, K., Anosova, M., Ntaflos, T., and Brandstätter, F. (2017) Enigmatic cathodoluminescent objects in the Dhofar 025 lunar meteorite: Origin and sources. Petrology, 25(2), 139-149.

Denevi, B.W., Koeber, S.D., Robinson, M.S., Garry, W.B., Hawke, B.R., Tran, T.N., Lawrence, S.J., Keszthelyi, L.P., Barnouin, O.S., and Ernst, C.M. (2012) Physical constraints on impact melt properties from Lunar Reconnaissance Orbiter Camera images. Icarus, 219(2), 665-675.

Dhingra, D., Pieters, C., Boardman, J., Head, J., Isaacson, P., and Taylor, L. (2011) Compositional diversity at Theophilus Crater: Understanding the geological context of Mg‐spinel bearing central peaks. Geophysical Research Letters, 38(11), L11201.

Dhingra, D., Pieters, C.M., Head, J.W., and Isaacson, P.J. (2013) Large mineralogically distinct impact melt feature at Copernicus crater–Evidence for retention of compositional heterogeneity. Geophysical Research Letters, 40(6), 1043-1048.

Dressler, B.O. (1984) The effects of the Sudbury event and the intrusion of the Sudbury Igneous Complex on the footwall rocks of the Sudbury Structure. The Geology and Ore Deposits of the Sudbury Structure. Edited by EG Pye, AJ Naldrett and PE Giblin. Ontario Geological Survey, Special, 1, 97-136.

Eckert, J.O.J., Taylor, L., and Neal, C. (1991) Spinel troctolite from Apollo 17 breccia 73215: Evidence for petrogenesis as deep-seated lunar crust. Lunar and Planetary Science Conference, 22, p. 329-332.

El Goresy, A. (1965) Baddeleyite and its significance in impact glasses. Journal of Geophysical Research, 70(14), 3453-3456.

Elardo, S.M., Draper, D.S., and Shearer, C.K. (2011) Lunar Magma Ocean crystallization revisited: Bulk composition, early cumulate mineralogy, and the source regions of the highlands Mg-suite. Geochimica et Cosmochimica Acta, 75(11), 3024-3045.

Elkins, L.T., Fernandes, V., Delano, J., and Grove, T. (2000) Origin of lunar ultramafic green glasses: Constraints from phase equilibrium studies. Geochimica et Cosmochimica Acta, 64(13), 2339-2350.

Elkins-Tanton, L.T., Burgess, S., and Yin, Q.-Z. (2011) The lunar magma ocean: Reconciling the solidification process with lunar petrology and geochronology. Earth and Planetary Science Letters, 304(3), 326-336.

Elkins-Tanton, L.T., Chatterjee, N., and Grove, T.L. (2003) Experimental and petrological constraints on lunar differentiation from the Apollo 15 green picritic glasses. Meteoritics & Planetary Science, 38(4), 515-527.

Finnila, A., Hess, P., and Rutherford, M. (1994) Assimilation by lunar mare basalts: Melting of crustal material and dissolution of anorthite. Journal of Geophysical Research: Planets, 99(E7), 14677-14690.

Ghiorso, M.S., Hirschmann, M.M., Reiners, P.W., and Kress, V.C. (2002) The pMELTS: A revision of MELTS for improved calculation of phase relations and major element partitioning related to partial melting of the mantle to 3 GPa. Geochemistry, Geophysics, Geosystems, 3(5), 1-35.

Ghiorso, M.S., and Sack, R.O. (1995) Chemical mass transfer in magmatic processes IV. A revised and internally consistent thermodynamic model for the interpolation and extrapolation of liquid-solid equilibria in magmatic systems at elevated temperatures and pressures. Contributions to Mineralogy and Petrology, 119(2-3), 197-212.

Glazner, A.F. (2007) Thermal limitations on incorporation of wall rock into magma. Geology, 35(4), 319-322.

Grieve, R.A.F., Dence, M.R., and Robertson, P.B. (1977) Cratering Processes: As Interpreted from the Occurrences of Impact Melts. In D.J. Roddy, R.O. Pepin, and R.B. Merrill, Eds. Impact and Explosion Cratering, p. 791-814. Pergamon, New York.

Gross, J., Isaacson, P.J., Treiman, A.H., Le, L., and Gorman, J.K. (2014) Spinel-rich lithologies in the lunar highland crust: Linking lunar samples with crystallization experiments and remote sensing. American Mineralogist, 99(10), 1849-1859.

Gross, J., and Treiman, A.H. (2011) Unique spinel‐rich lithology in lunar meteorite ALHA 81005: Origin and possible connection to M^3 observations of the farside highlands. Journal of Geophysical Research: Planets, 116, E10009.

Gualda, G.A., Ghiorso, M.S., Lemons, R.V., and Carley, T.L. (2012) Rhyolite-MELTS: a modified calibration of MELTS optimized for silica-rich, fluid-bearing magmatic systems. Journal of Petrology, 53(5), 875-890.

Haruyama, J., Matsunaga, T., Ohtake, M., Morota, T., Honda, C., Yokota, Y., Torii, M., Ogawa, Y., and Group, L.W. (2008) Global lunar-surface mapping experiment using the Lunar Imager/Spectrometer on SELENE. Earth, planets and space, 60(4), 243-255.

Herzberg, C.T. (1978) The bearing of spinel cataclasites on the crust-mantle structure of the moon. Lunar and Planetary Science Conference Proceedings, 9, p. 319-336.

-. (1983) The reaction forsterite + cordierite = aluminous orthopyroxene + spinel in the system MgO-Al_2O_3-SiO_2. Contributions to Mineralogy and Petrology, 84(1), 84-90.

Herzberg, C.T., and Baker, M.B. (1980) The cordierite-to spinel-cataclasite transition - Structure of the lunar crust. Proceedings of the Conference on the Lunar Highlands Crust, p. 113-132. Pergamon, New York.

Hess, P.C. (1994) Petrogenesis of lunar troctolites. Journal of Geophysical Research: Planets, 99(E9), 19083-19093.

Hörz, F. (1965) Untersuchungen an Riesgläsern. Contributions to Mineralogy and Petrology, 11(7), 621-661.

Huebner, J.S., and Turnock, A.C. (1980) The melting relations at 1 bar of pyroxenes composed largely of Ca-, Mg-, and Fe-bearing components. American Mineralogist, 65, 225-271.

Hurwitz, D.M., and Kring, D.A. (2014) Differentiation of the South Pole–Aitken Basin impact melt sheet: Implications for lunar exploration. Journal of Geophysical Research: Planets, 119(6), 1110-1133.

Irvine, T. (1974) Olivine-pyroxene-plagioclase relations in the system Mg_2SiO_4-$CaAl_2Si_2O_8$-$KAlSi_3O_8$-SiO_2 and their bearing on the differentiation of stratiform intrusions. Yearbook, Carnegie Institution Washington, 74, 492-500.

Jackson, C.R., Cheek, L.C., Williams, K.B., Hanna, K.D., Pieters, C.M., Parman, S.W., Cooper, R.F., Dyar, M.D., Nelms, M., and Salvatore, M.R. (2014) Visible-infrared spectral properties of iron-bearing aluminate spinel under lunar-like redox conditions. American Mineralogist, 99(10), 1821-1833.

James, O.B., and Hedenquist, J. (1978) Spinel-bearing troctolitic basalt 73215,170: Texture, mineralogy, and history. Lunar and Planetary Science Conference, 9, 588-590.

Jessberger, E. (1979) Ancient pink-spinel troctolitic basalt in Apollo 17 breccia 73215. Lunar and Planetary Science Conference, 10, p. 625-627.

Johnson, B.C., Minton, D.A., Melosh, H., and Zuber, M.T. (2015) Impact jetting as the origin of chondrules. Nature, 517(7534), 339-341.

Kaur, P., Chauhan, P., Bhattacharya, S., and Kumar, A. (2012) Compositional diversity at Tycho crater: Mg-Spinel exposures detected from Moon Mineralogical Mapper (M^3) data. Lunar and Planetary Science Conference, 43, p. Abstract #1434.

Kelemen, P.B. (1990) Reaction between ultramafic rock and fractionating basaltic magma I. Phase relations, the origin of calc-alkaline magma series, and the formation of discordant dunite. Journal of Petrology, 31(1), 51-98.

Kohut, E.J., and Nielsen, R.L. (2003) Low‐pressure phase equilibria of anhydrous anorthite‐bearing mafic magmas. Geochemistry, Geophysics, Geosystems, 4(7).

Korotev, R.L., Zeigler, R.A., and Floss, C. (2010) On the origin of impact glass in the Apollo 16 regolith. Geochimica et Cosmochimica Acta, 74(24), 7362-7388.

Kushiro, I., Ikeda, Y., and Nakamura, Y. (1972) Petrology of Apollo 14 high-alumina basalt. Proceedings of the Third Lunar Science Conference, p. 115-129.

Lal, D., Chauhan, P., Shah, R., Bhattacharya, S., and Kumar, A.K. (2012) Detection of Mg spinel lithologies on central peak of crater Theophilus using Moon Mineralogy Mapper (M^3) data from Chandrayaan-1. Journal of earth system science, 121(3), 847-853.

Libourel, G., Boivin, P., and Biggar, G.M. (1989) The univariant curve liquid = forsterite + anorthite + diopside in the system CMAS at 1 bar: solid solutions and melt structure. Contributions to Mineralogy and Petrology, 102(4), 406-421.

Lipin, B.R. (1978) System Mg_2SiO_4 - Fe_2SiO_4 - $CaAl_2Si_2O_8$ - SiO_2 and the origin of Fra Mauro basalts. American Mineralogist, 63(3), 350-364.

Longhi, J. (1987) Liquidus equilibria and solid solution in the system $CaAl_2Si_2O_8$-Mg_2SiO_4-$CaSiO_3$-SiO_2 at low pressure. American Journal of Science, 287(4), 265-331.

Longhi, J., Durand, S.R., and Walker, D. (2010) The pattern of Ni and Co abundances in lunar olivines. Geochimica et Cosmochimica Acta, 74(2), 784-798.

Lukas, H.L., Fries, S.G., and Sundman, B. (2007) Computational thermodynamics: The Calphad method. Cambridge University Press Cambridge, UK.

Marsh, B.D. (2013) On some fundamentals of igneous petrology. Contributions to Mineralogy and Petrology, 166(3), 665-690.

Marvin, U.B., Carey, J.W., and Lindstrom, M.M. (1989) Cordierite-spinel troctolite, a new magnesium-rich lithology from the lunar highlands. Science, 243(4893), 925-928.

Marvin, U.B., and Walker, D. (1985) A transient heating event in the history of a highlands troctolite from Apollo 12 soil 12033. Lunar and Planetary Science Conference Proceedings, 15, p. C421-C429.

McCallum, I. (1996) The Stillwater Somplex. In R. Cawthorne, Ed. Layered Intrusions: Developments in Petrology, 15, p. 441-483. Elsevier.

McCallum, I.S., and Schwartz, J.M. (2001) Lunar Mg suite: Thermobarometry and petrogenesis of parental magmas. Journal of Geophysical Research: Planets, 106(E11), 27969-27983.

McGee, P.E., Warner, J.L., and Simonds, C.H. (1977) Introduction to the Apollo collections. Part 1: Lunar igneous rocks. NASA STI/Recon Technical Report.

Mehta, S., and Goldstein, J.I. (1980) Metallic particles in the glassy constituents of three lunar highland samples 65315, 67435 and 78235. Proceedings of the Lunar and Planetary Science Conference, 11, 1713-1725.

Melosh, H.J. (1989) Impact Cratering: A Geologic Process. 245 p. Oxford University Press, Oxford, Great Britain.

Meyer, J., Elkins-Tanton, L., and Wisdom, J. (2010) Coupled thermal–orbital evolution of the early Moon. Icarus, 208(1), 1-10.

Milholland, C.S., and Presnall, D.C. (1998) Liquidus phase relations in the $CaO–MgO–Al_2O_3–SiO_2$ system at 3.0 GPa: the aluminous pyroxene thermal divide and high-pressure fractionation of picritic and komatiitic magmas. Journal of Petrology, 39(1), 3-27.

Morgan, Z., Liang, Y., and Hess, P. (2006) An experimental study of anorthosite dissolution in lunar picritic magmas: implications for crustal assimilation processes. Geochimica et Cosmochimica Acta, 70(13), 3477-3491.

Morse, S.A. (1980) Basalts and Phase Diagrams: An Introduction to the Quantitative Use of Phase Diagrams in Igneous Petrology. 493 p. Springer Verlag, New York

Naney, M., Crowl, D., and Papike, J. (1976) The Apollo 16 drill core - Statistical analysis of glass chemistry and the characterization of a high alumina-silica poor/HASP/glass. Lunar and Planetary Science Conference Proceedings, 7, p. 155-184.

Nazarov, M., Aranovich, L.Y., Demidova, S., Ntaflos, T., and Brandstätter, F. (2011) Aluminous enstatites of lunar meteorites and deep-seated lunar rocks. Petrology, 19(1), 13-25.

O'Keefe, J.D., and Ahrens, T.J. (1975) Shock effects from a large impact on the Moon. Proceedings of Lunar and Planetary Science Conference, 6, 2831-2844.

O'Keefe, J.D., and Ahrens, T.J. (1977) Impact-induced energy partitioning, melting, and vaporization on terrestrial planets. Proceedings of the Lunar and Planetary Science Conference, 8, 3357-3374.

Öhman, T., and Kring, D.A. (2012) Photogeologic analysis of impact melt‐rich lithologies in Kepler crater that could be sampled by future missions. Journal of Geophysical Research: Planets, 117(E12).

Osborn, E., and Tait, D. (1952) The system diopside-forsterite-anorthite. American Journal of Science, 38, 413-433.

Pan, V., and Longhi, J. (1990) The system Mg_2SiO_4-Ca_2SiO_4-$CaAl_2O_4$-$NaAlSiO_4$-SiO_2: One atmosphere liquidus equilibria of analogs of alkaline mafic lavas. Contributions to Mineralogy and Petrology, 105(5), 569-584.

Papike, J.J., Ryder, G., and Shearer Jr, C.K. (1998) Lunar Samples. In J.J. Papike, Ed. Planetary Materials, p. 1-234. Mineralogical Society of America, Washington DC.

Peale, S.J., Cassen, P., and Reynolds, R.T. (1979) Melting of Io by tidal dissipation. Science, 203(4383), 892-894.

Philpotts, A., and Ague, J. (2009) Principles of igneous and metamorphic petrology. Cambridge University Press.

Pieters, C.M., Besse, S., Boardman, J., Buratti, B., Cheek, L., Clark, R., Combe, J., Dhingra, D., Goswami, J., and Green, R. (2011) Mg-spinel lithology: A new rock type on the lunar farside. Journal of Geophysical Research: Planets, 116, E00G08.

Pieters, C.M., Goswami, J.N., Clark, R.N., Annadurai, M., Boardman, J., Buratti, B., Combe, J.-P., Dyar, M.D., Green, R., Head, J.W., Hibbits, C., Hicks, M., Isaacson, P., Klima, R., Kramer, G., Kumar, S., Livo, E., Lundeen, S., Malaret, E., McCord, T., Mustard, J., Nettles, J., Petro, N.E., Runyon, C., Staid, M., Sunshine, J., Taylor, L.A., Tompkins, S., and Varanasi, P. (2009) Character and spatial distribution of OH/H_2O on the surface of the Moon seen by M^3 on Chandrayaan-1. Science, 326(5952), 568-572.

Pieters, C.M., Hanna, K.D., Cheek, L., Dhingra, D., Prissel, T., Jackson, C., Moriarty, D., Parman, S., and Taylor, L.A. (2014) The distribution of Mg-spinel across the Moon and constraints on crustal origin. American Mineralogist, 99(10), 1893-1910.

Pittarello, L., and Koeberl, C. (2013) Petrography of impact glasses and melt breccias from the El'gygytgyn impact structure, Russia. Meteoritics & Planetary Science, 48(7), 1236-1250.

Powell, R., White, R., Green, E., Holland, T., and Diener, J. (2014) On parameterizing thermodynamic descriptions of minerals for petrological calculations. Journal of metamorphic Geology, 32(3), 245-260.

Presnall, D., Dixon, S.A., Dixon, J.R., O'Donnell, T., Brenner, N., Schrock, R., and Dycus, D. (1978) Liquidus phase relations on the join diopside-forsterite-anorthite from 1 atm to 20 kbar: their bearing on the generation and crystallization of basaltic magma. Contributions to Mineralogy and Petrology, 66(2), 203-220.

Prinz, M., Dowty, E., Keil, K., and Bunch, T. (1973) Spinel troctolite and anorthosite in Apollo 16 samples. Science, 179(4068), 74-76.

Prissel, T.C., and Gross, J. (2018) Re-examining the petrogenesis of lunar troctolites. Lunar and Planetary Science Conference, 49th, p. Abstr. #2583.

Prissel, T.C., Parman, S., Jackson, C., Rutherford, M., Hess, P., Head, J., Cheek, L., Dhingra, D., and Pieters, C. (2014) Pink Moon: The petrogenesis of pink spinel anorthosites and implications concerning Mg-suite magmatism. Earth and Planetary Science Letters, 403, 144-156.

Prissel, T.C., Parman, S.W., and Head, J.W. (2016a) Formation of the lunar highlands Mg-suite as told by spinel. American Mineralogist, 101(7), 1624-1635.

Prissel, T.C., Whitten, J.L., Parman, S.W., and Head, J.W. (2016b) On the potential for lunar highlands Mg-suite extrusive volcanism and implications concerning crustal evolution. Icarus, 277, 319-329.

Ridley, W., Reid, A., Warner, J., Brown, R., Gooley, R., and Donaldson, C. (1973) Glass compositions in Apollo 16 soils 60501 and 61221. Lunar and Planetary Science Conference Proceedings, 4, p. 309-321.

Riller, U., Lieger, D., Gibson, R.L., Grieve, R.A., and Stöffler, D. (2010) Origin of large-volume pseudotachylite in terrestrial impact structures. Geology, 38(7), 619-622.

Robinson, K., and Kring, D. (2018) The Northwest Africa 5744 Group: A Glimpse into Schrödinger-Like Lithologies? Lunar and Planetary Science Conference, 49.

Roedder, E. (1965) A laboratory reconaissance of the liquidus surface on the pyroxene system En-Di-Hd-Fs ($MgSiO_3$-$CaMgSi_2O_6$-$CaFeSi_2O_6$-$FeSiO_3$). American Mineralogist, 50, 696-703.

Ryder, G., and Ostertag, R. (1983) ALHA 81005: Moon, mars, petrography, and Giordano Bruno. Geophysical Research Letters, 10(9), 791-794.

Ryder, G., and Spudis, P. (1987) Chemical composition and origin of Apollo 15 impact melts. Journal of Geophysical Research: Solid Earth, 92(B4).

Saxena, S.K. (2010) Thermodynamic modeling of the Earth's interior. Elements, 6(5), 321-325.

Schairer, J.F. (1942) The system CaO ‐ FeO ‐ AI_2O_3 ‐ SiO_2: I, Results of quenching experiments on five joins. Journal of the American Ceramic Society, 25(10), 241-274.

Schmid-Fetzer, R. (2014) Phase diagrams: the beginning of wisdom. Journal of Phase Equilibria and Diffusion, 35(6), 735-760.

Sen, G. (2013) Petrology: Principles and Practice. Springer Science & Business Media.

Sen, G., and Presnall, D. (1984) Liquidus phase relationships on the join anorthite-forsterite-quartz at 10 kbar with applications to basalt petrogenesis. Contributions to Mineralogy and Petrology, 85(4), 404-408.

Shearer, C.K., Elardo, S.M., Petro, N.E., Borg, L.E., and McCubbin, F.M. (2015) Origin of the lunar highlands Mg-suite: An integrated petrology, geochemistry, chronology, and remote sensing perspective. American Mineralogist, 100(2), 294-325.

Shervais, J.W., Taylor, L.A., and Lindstrom, M.M. (1988) Olivine vitrophyres - A nonpristine high-Mg component in lunar breccia 14321. Proceedings Lunar and Planetary Science Conference 18, p. 45-57.

Simonds, C. (1975) Thermal regimes in impact melts and the petrology of the Apollo 17 Station 6 boulder. Lunar and Planetary Science Conference Proceedings, 6, p. 641-672.

Snape, J.F., Nemchin, A.A., Bellucci, J.J., and Whitehouse, M.J. (2017) Pb isotopes in the impact melt breccia 66095: Association with the Imbrium basin and the isotopic composition of lithologies at the Apollo 16 landing site. Chemical Geology, 466, 608-616.

Snyder, G.A., Taylor, L.A., and Halliday, A.N. (1995) Chronology and petrogenesis of the lunar highlands alkali suite: Cumulates from KREEP basalt crystallization. Geochimica et Cosmochimica Acta, 59(6), 1185-1203.

Sotin, C., Tobie, G., Wahr, J., McKinnon, W.B., McKinnon, W., and Khurana, K. (2009) Tides and tidal heating on Europa. In P.R. T, M.W. B, and K.K. K, Eds. Europa p. 85-118. University of Arizona Press, Tucson AZ.

Sparks, S.R., Sigurdsson, H., and Wilson, L. (1977) Magma mixing: a mechanism for triggering acid explosive eruptions. Nature, 267(5609), 315-318.

Stopar, J.D., Hawke, B.R., Robinson, M.S., Denevi, B.W., Giguere, T.A., and Koeber, S.D. (2014) Occurrence and mechanisms of impact melt emplacement at small lunar craters. Icarus, 243, 337-357.

Sun, Y., Li, L., and Zhang, Y. (2017) Detection of Mg-spinel bearing central peaks using M^3 images: Implications for the petrogenesis of Mg-spinel. Earth and Planetary Science Letters, 465, 48-58.

Takeda, H., Yamaguchi, A., Bogard, D., Karouji, Y., Ebihara, M., Ohtake, M., Saiki, K., and Arai, T. (2006) Magnesian anorthosites and a deep crustal rock from the farside crust of the moon. Earth and Planetary Science Letters, 247(3), 171-184.

Tian, Z., Wisdom, J., and Elkins-Tanton, L.T. (2017) Coupled orbital-thermal evolution of the early Earth-Moon system with a fast-spinning Earth. Icarus, 281, 90-102.

Timms, N.E., Erickson, T.M., Zanetti, M.R., Pearce, M.A., Cayron, C., Cavosie, A.J., Reddy, S.M., Wittmann, A., and Carpenter, P.K. (2017) Cubic zirconia in >2370° C impact melt records Earth's hottest crust. Earth and Planetary Science Letters, 477, 52-58.

Treiman, A.H., Gross, J., and Glazner, A.F. (2015) Lunar rocks rich in Mg-Al spinel: Enthalpy constraints suggest origins by impact melting. Lunar and Planetary Science Conference, 46, p. Abstract #2518.

Treiman, A.H., Maloy, A.K., Shearer, C.K., and Gross, J. (2010) Magnesian anorthositic granulites in lunar meteorites Allan Hills A81005 and Dhofar 309: Geochemistry and global significance. Meteoritics & Planetary Science, 45(2), 163-180.

Ussler, W., and Glazner, A.F. (1992) Graphical analysis of enthalpy-composition relationships in mixed magmas. Journal of volcanology and geothermal research, 51(1), 23-40.

Vaughan, W.M., Head, J.W., Wilson, L., and Hess, P.C. (2013) Geology and petrology of enormous volumes of impact melt on the Moon: A case study of the Orientale basin impact melt sea. Icarus, 223(2), 749-765.

Walker, D., Longhi, J., Grove, T.L., Stolper, E., and Hays, J.F. (1973) Experimental petrology and origin of rocks from the Descartes Highlands. Lunar and Planetary Science Conference Proceedings, 4, p. 1013-1032.

Walton, E., Hughes, A., MacLagan, E., Herd, C., and Dence, M. (2017) A previously unrecognized high-temperature impactite from the Steen River impact structure, Alberta, Canada. Geology, 45(4), 291-294.

Warren, P.H. (1986) Anorthosite assimilation and the origin of the Mg/Fe‐related bimodality of pristine moon rocks: Support for the magmasphere hypothesis. Journal of Geophysical Research: Solid Earth, 91(B4), 331-343.

Warren, P.H., Taylor, G.J., Keil, K., Kallemeyn, G.W., Rosener, P.S., and Wasson, J.T. (1983) Sixth foray for pristine nonmare rocks and an assessment of the diversity of lunar anorthosites. Journal of Geophysical Research: Solid Earth, 88(S02).

Williams, K.B., Jackson, C.R., Cheek, L.C., Donaldson-Hanna, K.L., Parman, S.W., Pieters, C.M., Dyar, M.D., and Prissel, T.C. (2016) Reflectance spectroscopy of chromium-bearing spinel with application to recent orbital data from the Moon. American Mineralogist, 101(3), 726-734.

Wiser, N.M., and Wood, B.J. (1991) Experimental determination of activities in Fe−Mg olivine at 1400 K. Contributions to Mineralogy and Petrology, 108(1), 146-153.

Yoder, H.S.J. (1975) Heat of melting of simple systems related to basalts and eclogites. Carnegie Inst. Washington Yrbk., 74, 515-519.

-. (1976) Generation of Basaltic Magma. 265 p. National Academies of Science.

Zieg, M.J., and Marsh, B.D. (2005) The Sudbury Igneous Complex: Viscous emulsion differentiation of a superheated impact melt sheet. Geological Society of America Bulletin, 117(11-12), 1427-1450.

This is a preprint, the final version is subject to change, of the American Mineralogist (MSA)
Cite as Authors (Year) Title. American Mineralogist, in press.
DOI: https://doi.org/10.2138/am-2019-6652

Table 1. Please see separate file

Table 2a. Chemical Components and Abbreviations

Component	Abbrev.	Composition
Anorthite	An	$CaAl_2Si_2O_8$
Forsterite	Fo	Mg_2SiO_4
Silica	Sil	SiO_2
Diopside	Di	$CaMgSi_2O_6$
Wollastonite	Wo	$CaSiO_3$
Ferrous Oxide	FeO	FeO

Table 2b. Phases and Abbreviations

Phase	Abbrev.	Composition[a]
Melt	L	Variable
Plagioclase	Pl	$CaAl_2Si_2O_8$
Olivine	Ol	$(Mg,Fe)_2SiO_4$
Spinel	Sp	$(Mg,Fe)Al_2O_4$
'Enstatite' [b]	Mpx	$(Mg,Fe,Ca)SiO_3$
Protopyroxene	PPx	$(Mg,Fe,Ca)SiO_3$
Pigeonite	Pig	$(Mg,Fe,Ca)SiO_3$
Orthopyroxene	OPx	$(Mg,Fe,Ca)SiO_3$
Ca-Pyroxene	Aug	$Ca(Mg,Fe)Si_2O_6$
Cordierite	Crd	$Mg_2Al_3(Si_5AlO_{18})$
Sapphirine	Sph	$Mg_4Al_{10}Si_2O_{13}$
Quartz	Q	SiO_2
Tridymite	Tr	SiO_2
Cristobalite	Crs	SiO_2
Immiscible Liquids	2L	Variable

[a] Ignores minor solid solutions, like Al in pyroxenes and olivine, Mg and Fe in plagioclase, and vacancies in spinel.
[b] Used for low-Ca pyroxenes when structure state is either not specified or not known.

This is a preprint, the final version is subject to change, of the American Mineralogist (MSA)
Cite as Authors (Year) Title. American Mineralogist, in press.
DOI: https://doi.org/10.2138/am-2019-6652

Table 1. Basalt and Peridotite Compositions used in Modeling

	Ideal	Natural Compositions		Projected into Fo-An-Di-Sil-FeO			Projected into Fo-An-Di-Sil			Projected into Fo-An-Sil[d]		
	Anorthite	A14grB[a]	MgSPM[b]	A14B	MgSPM	Perid14B[c]	A14B'	MgSPM'	Perid14B'[c]	A14B"	MgSPM"	Perid14B"[c]
SiO_2	43.19	44.80	44.03	45.00	44.58	45.4	49.42	45.69	51.1	48.09	44.78	49.81
TiO_2	0.00	0.45	0.93	0.00	0.00	0.00	0.00	0.00	0.00	0.00	0.00	0.00
Al_2O_3	36.65	7.14	17.35	7.11	18.07	0.00	7.81	18.52	0.00	9.50	20.46	0.00
Cr_2O_3	0.00	0.54	0.36	0.00	0.00	0.00	0.00	0.00	0.00	0.00	0.00	0.00
FeO	0.00	19.80	4.74	20.34	5.53	25.2	0.00	0.00	0.00	0.00	0.00	0.00
MnO	0.00	0.24	0.21	0.00	0.00	0.00	0.00	0.00	0.00	0.00	0.00	50.19
MgO	0.00	19.10	16.72	19.39	18.67	24.1	33.82	22.31	43.0	37.15	23.42	0.00
CaO	20.16	8.03	11.78	8.15	13.15	5.30	8.95	13.48	5.9	5.24	11.28	0.00
Na_2O	0.00	0.06	0.4	0.00	0.00	0.00	0.00	0.00	0.00	0.00	0.00	0.00
K_2O	0.00	0.03	0.464	0.00	0.00	0.00	0.00	0.00	0.00	0.00	0.00	0.00
sum	100.	100.19	96.98	100.	100.	100.	100.	100.	100.	100.	100.	100.
Norm	Wt%											
Pl	100	19.6	49.0	21.3	50.5	0.0	21.3	50.5	0.0	26.0	56.0	0
Ol	0	35.5	26.6	35.6	30.3	45.2	35.6	30.3	45.2	43.3	33.5	58.6
Hy	0	26.2	7.6	25.2	6.5	32.0	25.2	6.5	32.0	30.7	10.5	41.4
Di	0	16.9	11.7	18.0	12.7	22.8	18.0	12.7	22.8	0	0	0
Or	0	0.2	2.8	0	0	0	0	0	0	0	0	0
Il	0	0.8	1.8	0	0	0	0	0	0	0	0	0
Chr	0	0.8	0.5	0	0	0	0	0	0	0	0	0
Mg*	--	63.2	86.3	63.2	86.3	63	100	100	100	100	100	100
An*	100	97.3	92.5	100	100	100	100	100	100	100	100	100

[a] Apollo 14 Green Glass B: Delano (1986), Elkins et al. (2000).
[b] "Mg-Suite Parent Magma" estimate: Longhi et al. (2010), Prissel et al. (2016).
[c] Peridotite compositions, projections of the natural compositions from An component onto An-free joins.
[d] See Supplemental Material.

DOI: https://doi.org/10.2138/am-2019-6652

REFERENCES

Delano, J.W. (1986) Pristine lunar glasses: Criteria, data, and implications. Journal of Geophysical Research: Solid Earth, 91(B4), 201-213.

Elkins, L., Fernandes, V., Delano, J., and Grove, T. (2000) Origin of lunar ultramafic green glasses: Constraints from phase equilibrium studies. Geochimica et Cosmochimica Acta, 64(13), 2339-2350.

Longhi, J., Durand, S.R., and Walker, D. (2010) The pattern of Ni and Co abundances in lunar olivines. Geochimica et Cosmochimica Acta, 74(2), 784-798.

Prissel, T.C., Parman, S.W., and Head, J.W. (2016) Formation of the lunar highlands Mg-suite as told by spinel. American Mineralogist, 101(7), 1624-1635.

This is a preprint, the final version is subject to change, of the American Mineralogist (MSA)
Cite as Authors (Year) Title. American Mineralogist, in press.
DOI: https://doi.org/10.2138/am-2019-6652

Figures: REVISION 1

Figure 1.

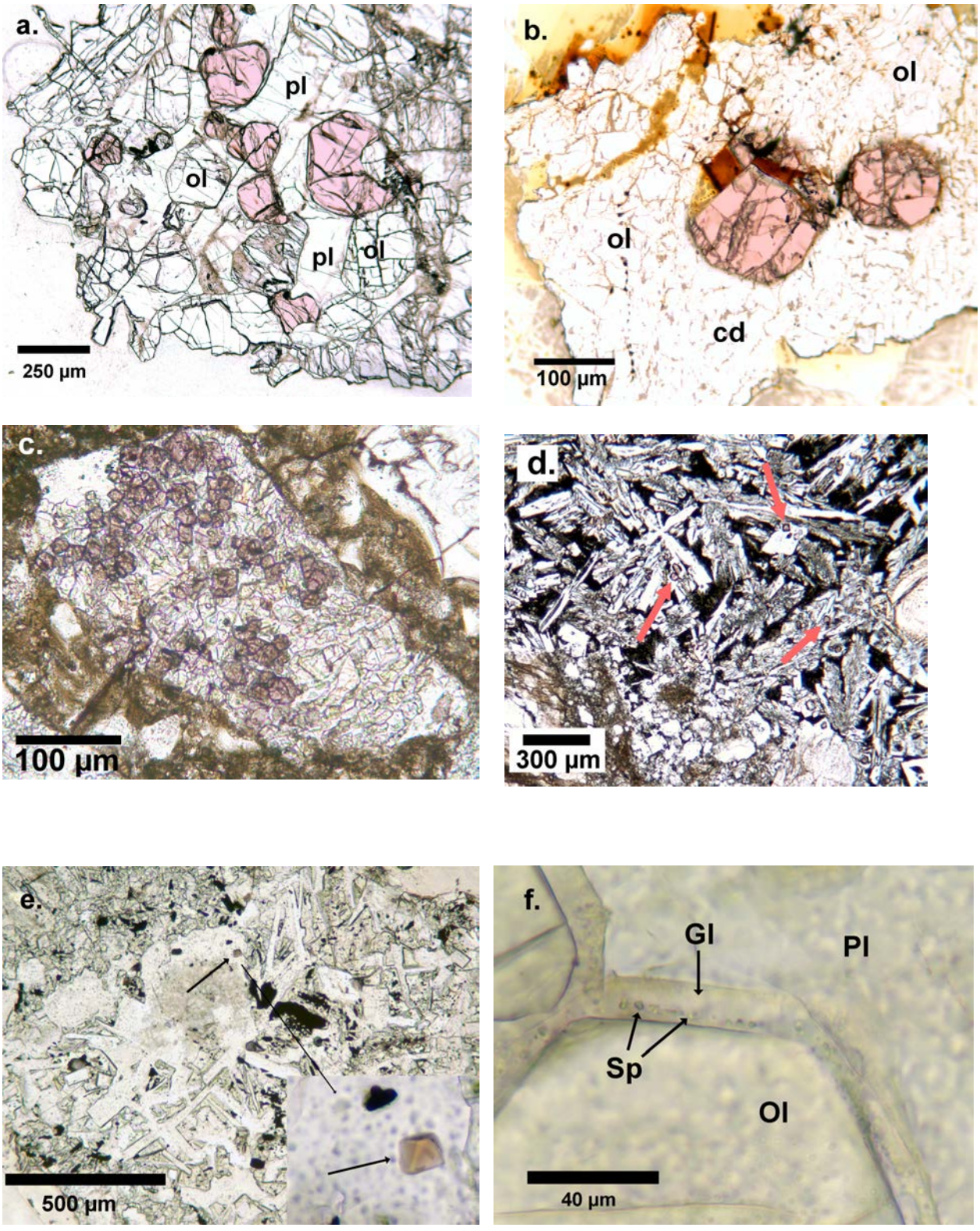

Figure 1. Lunar Spinels in Thin Section, all in plane-polarized light.

a. Cumulate igneous troctolite 67435 (Prinz et al., 1973). Pink spinel and clear olivine (ol, higher relief) enclosed poikilitically by plagioclase (pl).

b. Cordierite-spinel troctolite 15295,100 (Marvin et al., 1989). Pink spinel euhedra embedded in olivine (ol, clear) and cordierite (cd, also clear). Yellow and brown colors are burnt epoxy, caused by exposure to electron beams.

c. Spinel-rich cumulate, meteorite ALH81005, clast 2 of Gross and Treiman (2011). Small purple spinel euhedra surrounded by olivine, plagioclase, and pyroxene.

d. Impact melt breccia 62295. Small purple spinel euhedra (arrows) in colorless plagioclase euhedra (Walker et al., 1973). Unmelted rock fragments to bottom middle and left. Image c/o Amy Fagan & LPI.

e. Anorthositic impact melt clast in in Apollo 12 regolith 12033,618. Euhedral spinel crystal (arrow) enclosed in plagiocase; inset is higher magnification view of the crystal, showing its octahedral shape. Other phases include pyroxene and ilmenite.

f. Partially melted troctolite clast in Apollo 12 regolith sample 12033,618 (Marvin and Walker, 1985), with tiny spinel euhedra (Sp) in glass (Gl, formerly impact melt) between plagioclase (Pl) and olivine (Ol).

This is a preprint, the final version is subject to change, of the American Mineralogist (MSA)
Cite as Authors (Year) Title. American Mineralogist, in press.
DOI: https://doi.org/10.2138/am-2019-6652

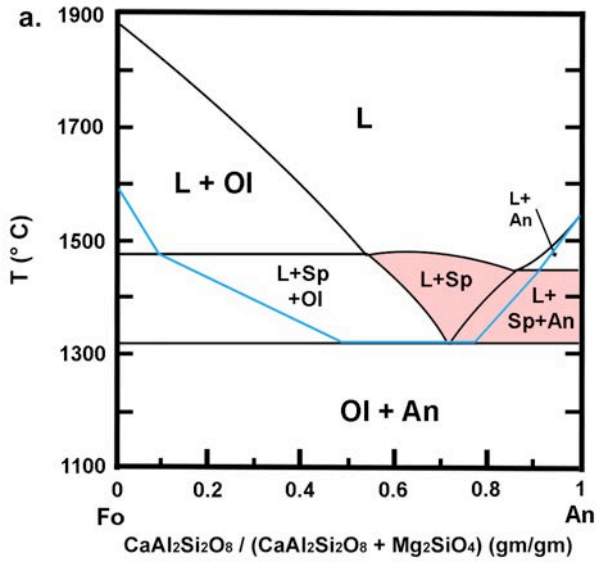

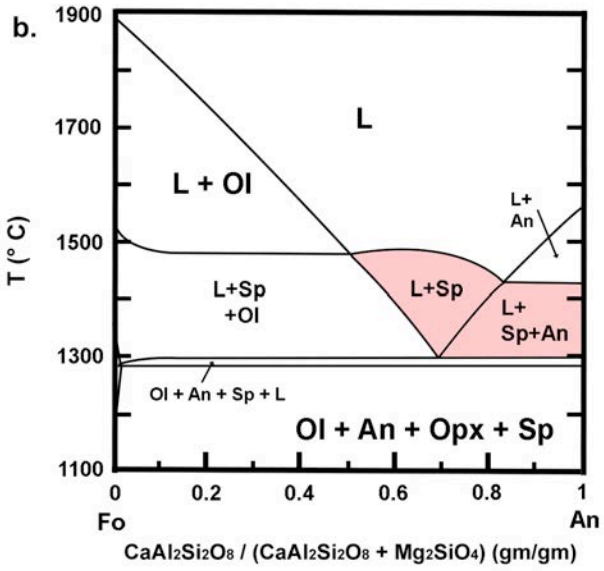

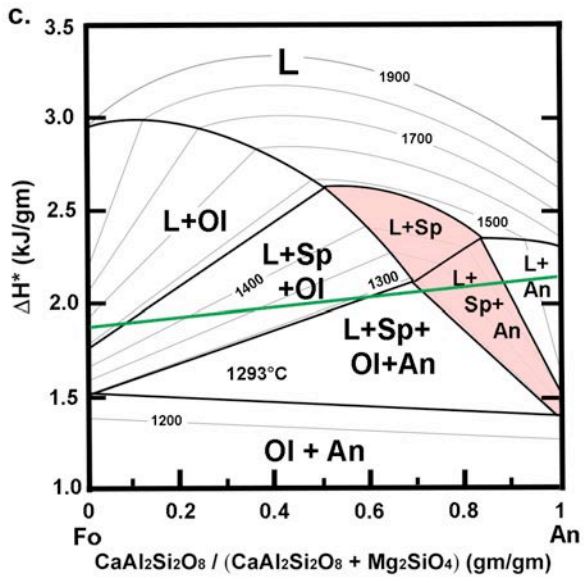

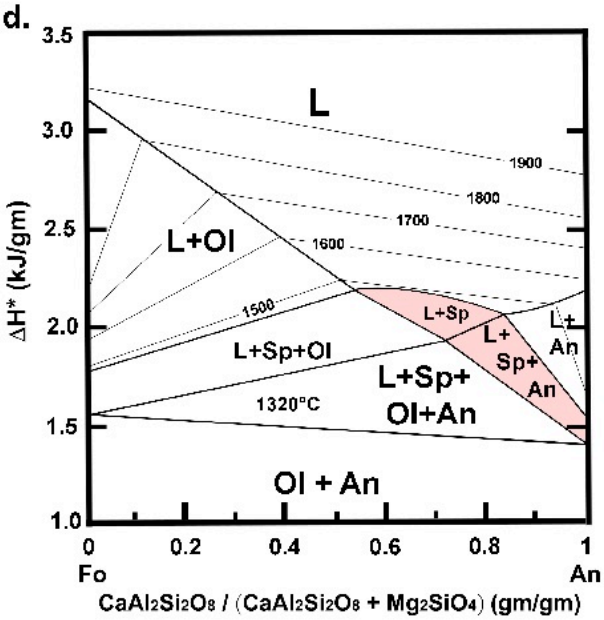

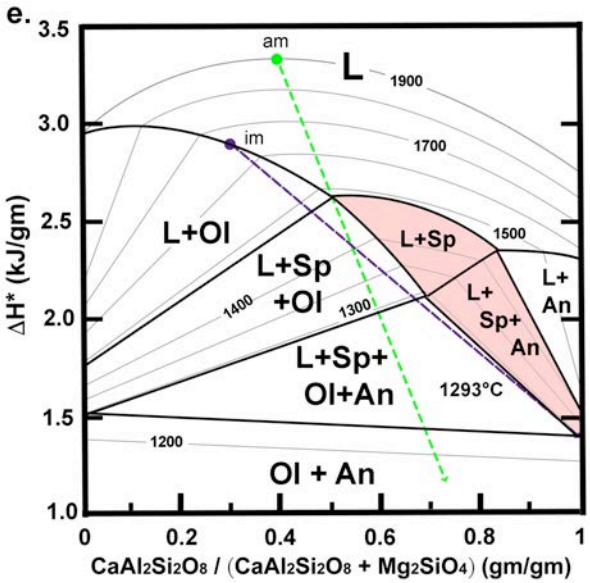

Figure 2. Phase equilibria in Mg_2SiO_4 – $CaAl_2Si_2O_8$ (Forsterite-Anorthite, Fo-An). ΔH^* defined in equation (1). Pink areas are phase fields that could appear as spinel-anorthosite, i.e. that include only Sp ± Pl ± L.

a. Temperature-composition (T-X) relations, from Osborn and Tait (1952). In the spinel-bearing fields, the compositions of the spinel and melt are outside this join. The spinel-out reaction at 1320°C is peritectic (monoresportional), and represents L + Sp = Ol + Pl. Blue line corresponds to ΔH^*= 1.9 kJ/mol in Figure 2c, and is clearly not isothermal.

b. T-X relations as calculated by FactSage (Bale et al., 2009; Bale et al., 2016). The geometry and locations of phase boundaries are essentially as determined in experiments, except that the calculated temperature of the L + Sp + Ol + Pl peritectic reaction is ~25°C lower than reported from experiments (Fig. 2a). FactSage includes non-idealities in the compositions of plagioclase, spinel, and olivine, which lead to the presence here of: complexities near Ol composition, the field of L+Sp+Ol+An, and the presence of Opx in the subsolidus region. These complexities are ignored in Figure 2c and further.

c. ΔH^*-X relations calculated with FactSage (Bale et al., 2009; Bale et al., 2016). The peritectic point on the T-X diagram appears as a broad field on the ΔH^*-X diagam, because significant heat is released in the crystallization of Ol + Pl. The calculated peritectic temperature, 1293°C, is lower than experimentally determined. Note that temperature is not conserved during mixing – the green line joins forsterite olivine at 1550°C with anorthite plagioclase at 1550°C; temperatures of mixtures along this line wiithout addition/removal of heat) range down to that of the peritectic.

d. Enthalpy-composition relations, calculated from the T-X phase diagram following Ussler and Glazner (1992). The geometry of the phase diagram is identical to that of the FactSage

This is a preprint, the final version is subject to change, of the American Mineralogist (MSA)
Cite as Authors (Year) Title. American Mineralogist, in press.
DOI: https://doi.org/10.2138/am-2019-6652

method (Figure 2c); all phase boundaries are linear because of the assumptions of ideal mixing in solids and silicate melt solution.

e. Annotated ΔH*-X diagram of **c**. Mixing an arbitrary melt composition, **am**, with anorthite in areas right of the green line can yield 'spinel anorthosite' (i.e, anorthite at nearly any ΔH* or T). Mixing an igneous melt composition, **im** (i.e., on the olivine liquidus surface), with anorthite can yield 'spinel anorthosite' only for regions to the right of the purple line, i.e. if the anorthite has ΔH* > 1.4 kJ/gm (at T > ~1300°C). See text.

This is a preprint, the final version is subject to change, of the American Mineralogist (MSA)
Cite as Authors (Year) Title. American Mineralogist, in press.
DOI: https://doi.org/10.2138/am-2019-6652

Figure 3.

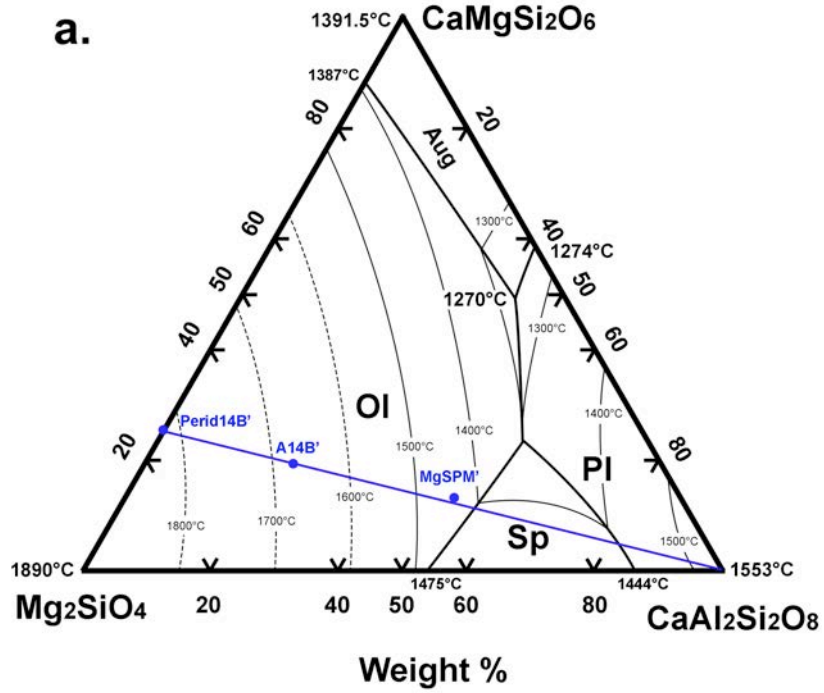

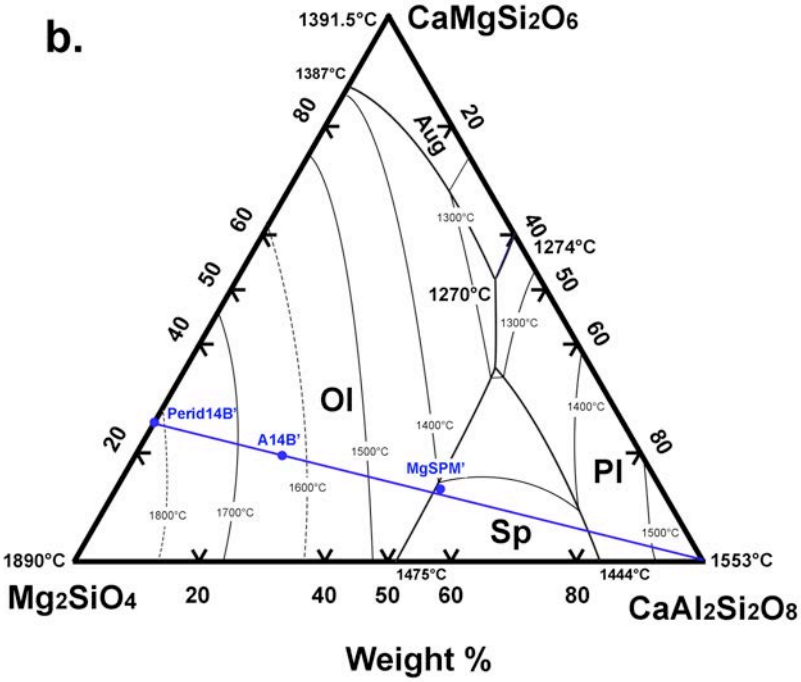

This is a preprint, the final version is subject to change, of the American Mineralogist (MSA)
Cite as Authors (Year) Title. American Mineralogist, in press.
DOI: https://doi.org/10.2138/am-2019-6652

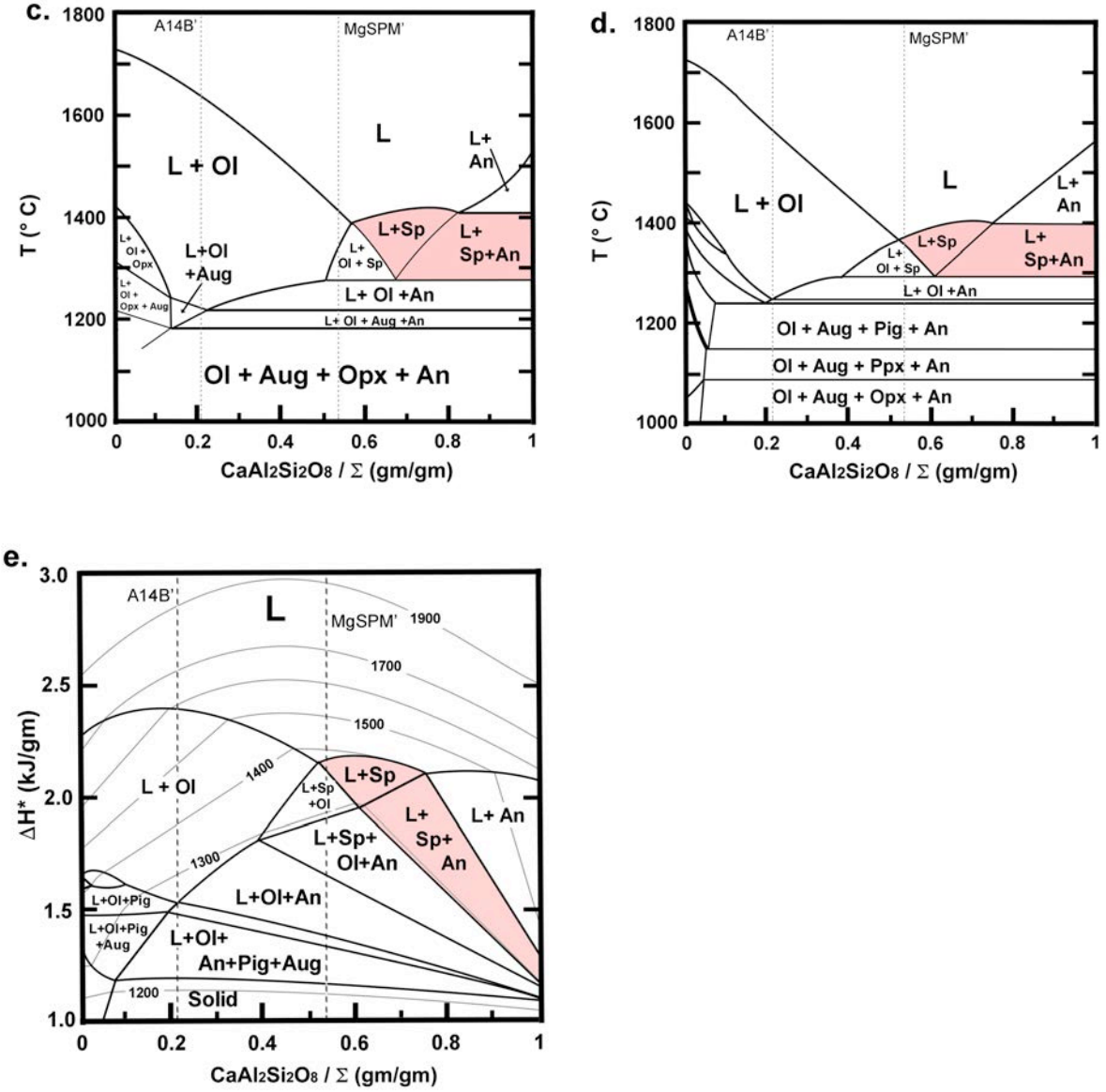

Figure 3. Phase relations in Mg_2SiO_4 – $CaAl_2Si_2O_8$ – $CaMgSi_2O_6$ – SiO_2, Forsterite-Anorthite-Diopside-Silica, Fo-An-Di-Qz. ΔH* defined in equation (1). Pink fields in parts c-f show phase fields that could appear as spinel-anorthosite, i.e. that include only Sp ± Pl ± L.

a. Ternary liquidus surface of Fo-An-Di (Osborn and Tait, 1952; Presnall et al., 1978; Biggar and Humphries, 1981; Libourel et al., 1989) Blue line is projection of the Perid14B'-An join; labeled blue point are projections of the lunar picrite composition A14B', and an inferred (Fe-free) parent magma for Mg-suite magmas, MgSPM', see Table 1 (Longhi et al., 2010).

b. Ternary liquidus surface of Fo-An-Di calculated in FactSage (Bale et al., 2009; Bale et al., 2016). Note that the liquidus field for spinel is larger than in experiments.

c. T-X phase diagram for the join Perid14B'-An (in Fo-An-Di-Qz); equilibrium phase boundary locations are a combination of those extrapolated from experiments and the Rhyolite-MELTS model.

d. T-X phase diagram for the pseudo-binary join Perid14B'-An (in Fo-An-Di-Qz), calculated from FactSage. The complex geometry of the lower left area (low T and An content) is shown in Supplement E, Figure E1.

e. ΔH^*-X diagram for the pseudo-binary join Perid14B'-An calculated with FactSage (Bale et al., 2009; Bale et al., 2016) consistent with Fig. 3d. The complex phase relations at lower T and lower An content (mostly involving pyroxenes) are omitted; see Appendix A.

This is a preprint, the final version is subject to change, of the American Mineralogist (MSA)
Cite as Authors (Year) Title. American Mineralogist, in press.
DOI: https://doi.org/10.2138/am-2019-6652

Figure 4.

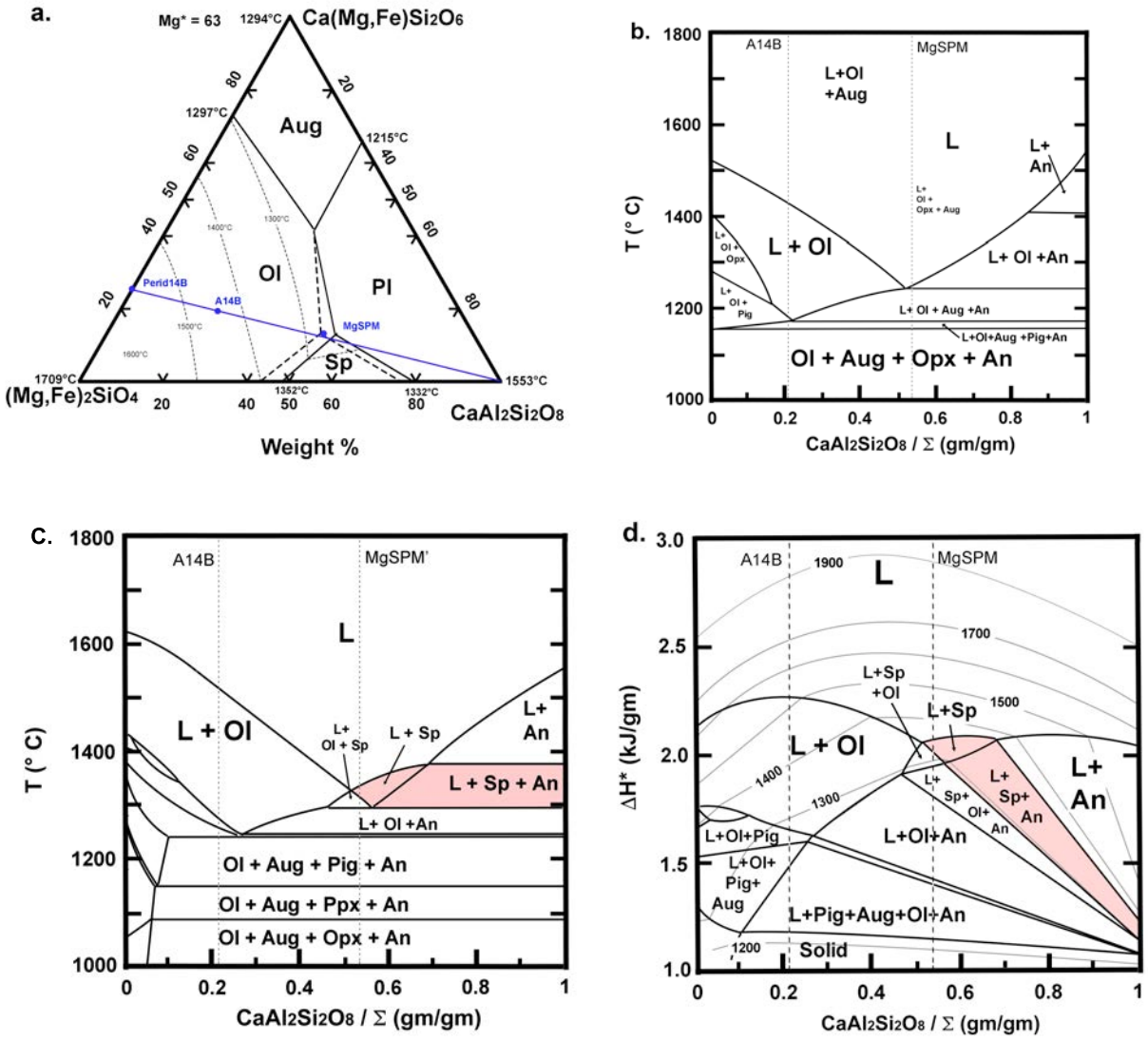

Figure 4. Phase relations in Mg_2SiO_4 – $CaAl_2Si_2O_8$ – $CaMgSi_2O_6$ – FeO – SiO_2, Forsterite-Anorthite-Diopside-FeO-Silica, Fo-An-Di-FeO-Qz, for Mg# = 63%. ΔH* defined in equation (1). Pink fields show phase fields that could appear as spinel-anorthosite, i.e. that include only Sp ± Pl ± L.

a. Liquidus surface for Forsterite-Anorthite-Diopside-FeO for Mg# = 63%. Liquidus cotectics and peritectics in heavy lines; solid as calculated by Rhyolite-MELTS (Gualda et al., 2012),

and dashed lines as extrapolated from experimental data of: Osborn and Tait (1952) for Mg# = 100%, Lipin (1978) for Mg# = 59%, Walker et al. (1973) for Mg# = 30%, and Schairer (1942) for Mg#=0%, Bowen and Schairer (1935), Roedder (1965), and Huebner and Turnock (1980). The calculated liquidus locations are within ~25°C of the few relevant experimental determinations (e.g. for the olivine-augite and olivine-plagioclase joins). Blue line is projection of the Perid14B-An join; labeled blue point are projections of the lunar picrite composition A14B, and an inferred (Fe-free) parent magma for Mg-suite magmas, MgSPM, see Table 1 (Longhi et al., 2010).

b. T-X phase relations along the pseudo-binary join Perid14B-Anorthite from Rhyolite-MELTS calculations, showing that spinel is not calculated to form along the join. The Perid14B composition (Mg#=63%) contains more SiO_2 than the olivine-augite join in Figure 4a. Thus, compared to Figure 4a, the diagram here has lower liquidus temperatures, appearance of low-Ca pyroxenes in the sub-liquidus, and the absence of spinel.

c. T-X phase relations along the pseudo-binary join Perid14B-Anorthite, as calculated with FactSage. The complex geometry at lower T and lower An content are omitted.

d. ΔH^*-X diagram for the pseudo-binary join Perid14B-An calculated with FactSage, consistent with Fig. 4c. The complex geometry at lower ΔH^* and lower An content are shown in Appendix A, Figure A4.

NOTE: The references for figures will be merged with those of the main text when the manuscript is accepted for publication.

References for Figures

Bale, C., Bélisle, E., Chartrand, P., Decterov, S., Eriksson, G., Gheribi, A., Hack, K., Jung, I.-H., Kang, Y.-B., and Melançon, J. (2016) FactSage thermochemical software and databases, 2010–2016. Calphad, 54, 35-53.

Bale, C., Bélisle, E., Chartrand, P., Decterov, S., Eriksson, G., Hack, K., Jung, I.-H., Kang, Y.-B., Melançon, J., and Pelton, A. (2009) FactSage thermochemical software and databases—recent developments. Calphad, 33(2), 295-311.

Biggar, G., and Humphries, D. (1981) The plagioclase, forsterite, diopside, liquid equilibrium in the system CaO-Na_2O-MgO-Al_2O_3-SiO_2. Mineralogical Magazine, 44, 309-314.

Bowen, N.L., and Schairer, J.F. (1935) The system MgO-FeO-SiO_2. American Journal of Science(170), 151-217.

Gross, J., and Treiman, A.H. (2011) Unique spinel ‐ rich lithology in lunar meteorite ALHA 81005: Origin and possible connection to M^3 observations of the farside highlands. Journal of Geophysical Research: Planets, 116, E10009.

Gualda, G.A., Ghiorso, M.S., Lemons, R.V., and Carley, T.L. (2012) Rhyolite-MELTS: a modified calibration of MELTS optimized for silica-rich, fluid-bearing magmatic systems. Journal of Petrology, 53(5), 875-890.

Huebner, J.S., and Turnock, A.C. (1980) The melting relations at 1 bar of pyroxenes composed largely of Ca-, Mg-, and Fe-bearing components. American Mineralogist, 65, 225-271.

Libourel, G., Boivin, P., and Biggar, G.M. (1989) The univariant curve liquid = forsterite + anorthite + diopside in the system CMAS at 1 bar: solid solutions and melt structure. Contributions to Mineralogy and Petrology, 102(4), 406-421.

Lipin, B.R. (1978) System Mg_2SiO_4 - Fe_2SiO_4 - $CaAl_2Si_2O_8$ - SiO_2 and the origin of Fra Mauro basalts. American Mineralogist, 63(3), 350-364.

Longhi, J., Durand, S.R., and Walker, D. (2010) The pattern of Ni and Co abundances in lunar olivines. Geochimica et Cosmochimica Acta, 74(2), 784-798.

Marvin, U.B., Carey, J.W., and Lindstrom, M.M. (1989) Cordierite-spinel troctolite, a new magnesium-rich lithology from the lunar highlands. Science, 243(4893), 925-928.

Marvin, U.B., and Walker, D. (1985) A transient heating event in the history of a highlands troctolite from Apollo 12 soil 12033. Lunar and Planetary Science Conference Proceedings, 15, p. C421-C429.

Osborn, E., and Tait, D. (1952) The system diopside-forsterite-anorthite. American Journal of Science, 38, 413-433.

Presnall, D., Dixon, S.A., Dixon, J.R., O'Donnell, T., Brenner, N., Schrock, R., and Dycus, D. (1978) Liquidus phase relations on the join diopside-forsterite-anorthite from 1 atm to 20 kbar: their bearing on the generation and crystallization of basaltic magma. Contributions to Mineralogy and Petrology, 66(2), 203-220.

Prinz, M., Dowty, E., Keil, K., and Bunch, T. (1973) Spinel troctolite and anorthosite in Apollo 16 samples. Science, 179(4068), 74-76.

Roedder, E. (1965) A laboratory reconaissance of the liquidus surface on the pyroxene system En-Di-Hd-Fs ($MgSiO_3$-$CaMgSi_2O_6$-$CaFeSi_2O_6$-$FeSiO_3$). American Mineralogist, 50, 696-703.

Schairer, J.F. (1942) The system CaO – FeO – Al_2O_3 – SiO_2: I, Results of quenching experiments on five joins. Journal of the American Ceramic Society, 25(10), 241-274.

Ussler, W., and Glazner, A.F. (1992) Graphical analysis of enthalpy-composition relationships in mixed magmas. Journal of volcanology and geothermal research, 51(1), 23-40.

Walker, D., Longhi, J., Grove, T.L., Stolper, E., and Hays, J.F. (1973) Experimental petrology and origin of rocks from the Descartes Highlands. Lunar and Planetary Science Conference Proceedings, 4, p. 1013-1032.